Springer Theses
Recognizing Outstanding Ph.D. Research

Yonatan Cohen

A New Platform for Edge Mode Manipulations in the Quantum Hall Effect

Springer

Springer Theses

Recognizing Outstanding Ph.D. Research

Aims and Scope

The series "Springer Theses" brings together a selection of the very best Ph.D. theses from around the world and across the physical sciences. Nominated and endorsed by two recognized specialists, each published volume has been selected for its scientific excellence and the high impact of its contents for the pertinent field of research. For greater accessibility to non-specialists, the published versions include an extended introduction, as well as a foreword by the student's supervisor explaining the special relevance of the work for the field. As a whole, the series will provide a valuable resource both for newcomers to the research fields described, and for other scientists seeking detailed background information on special questions. Finally, it provides an accredited documentation of the valuable contributions made by today's younger generation of scientists.

Theses are accepted into the series by invited nomination only and must fulfill all of the following criteria

- They must be written in good English.
- The topic should fall within the confines of Chemistry, Physics, Earth Sciences, Engineering and related interdisciplinary fields such as Materials, Nanoscience, Chemical Engineering, Complex Systems and Biophysics.
- The work reported in the thesis must represent a significant scientific advance.
- If the thesis includes previously published material, permission to reproduce this must be gained from the respective copyright holder.
- They must have been examined and passed during the 12 months prior to nomination.
- Each thesis should include a foreword by the supervisor outlining the significance of its content.
- The theses should have a clearly defined structure including an introduction accessible to scientists not expert in that particular field.

More information about this series at http://www.springer.com/series/8790

Yonatan Cohen

A New Platform for Edge Mode Manipulations in the Quantum Hall Effect

Doctoral Thesis accepted by the Weizmann Institute of Science, Rehovot, Israel

Springer

Author
Dr. Yonatan Cohen
Braun Center for Submicron Research
Weizmann Institute of Science
Rehovot, Israel

Supervisor
Prof. Moty Heiblum
Braun Center for Submicron Research
Weizmann Institute of Science
Rehovot, Israel

ISSN 2190-5053 ISSN 2190-5061 (electronic)
Springer Theses
ISBN 978-3-030-05942-2 ISBN 978-3-030-05943-9 (eBook)
https://doi.org/10.1007/978-3-030-05943-9

Library of Congress Control Number: 2018964231

This Springer imprint is published by the registered company Springer Nature Switzerland AG
The registered company address is: Gewerbestrasse 11, 6330 Cham, Switzerland

To my grandma

Supervisor's Foreword

Quantum topological systems are characterized by a bulk gap and gapless edge modes, which can carry charge, spin, and energy. The low-energy dynamics of such systems is dictated by the edge. Consequently, any application of such systems to quantum transport, to quantum information processing, or to the design of quantum devices, necessitates a good understating of their edge structure, its robustness against small perturbations, and its dependence on the system characteristics.

The quantum Hall effect (QHE) is the archetype of topological states. While edge physics in the QHE regime has been a focal theme over nearly three decades, recent experimental observations demonstrate that there are fundamental facets of QHE edge physics that are far from being understood. A few examples are: (i) Combined measurements of complex and even simpler filling factors are not consistent with the minimal edge structure that is usually employed for the edge, hence requiring edge reconstruction to explain the observations. (ii) According to the standard picture of edge states, elementary excitations along the edge involve fractionally charged anyons. These anyons possess fractional exchange statistics (intermediate between bosons and fermions) and may even support non-abelian quasiparticles. However, notwithstanding long, extensive efforts, to detect anyonic interference remains evasive. (iii) In contrast to the standard picture of edge states in the QHE regime, it was found experimentally that neutral modes are much more abundant than theoretically expected. Moreover, their quantum nature (e.g., amenability to quantum interference) is not understood.

The work describes a new method to produce on-demand complex 1D mode structures. The complex chiral modes, integer or fractional, "helical" or spinful, can be adeptly controlled, with their inter-mode equilibration tuned by gating or magnetic field. This also means that they provide a readily available experimental laboratory to test novel theoretical ideas of a rich menu of edge structures, avoiding the pitfalls of structural and dynamical unknowns at the edge (which may lead to ambiguous and confusing insights). This novel synthetic chiral modes can be

employed as a platform for novel tests of the **fundamentals of quantum mechanics** (e.g., the Aharonov–Casher effect, interference between electrons and anyons), and for engineering of new exotic zero modes for use in **topological quantum computation**.

Rehovot, Israel
September 2018

Prof. Moty Heiblum

Abstract

Electronic systems harboring one-dimensional helical modes, where spin and momentum are locked, have lately become an important field of its own. When coupled to a conventional superconductor, such systems are expected to manifest topological superconductivity, a unique phase hosting exotic Majorana zero modes. Even more interesting are fractional helical modes, yet to be observed, which open the route for realizing generalized parafermionic zero modes. Possessing non-abelian exchange statistics, these quasiparticles may serve as building blocks in topological quantum computing. Here, we present a new approach to form protected one-dimensional helical edge modes in the quantum Hall regime. The novel platform is based on a carefully designed double-quantum-well structure in a GaAs-based system hosting two electronic sub-bands; each tuned to the quantum Hall effect regime. By electrostatic gating of different areas of the structure, counter-propagating integer, as well as fractional, edge modes with opposite spins are formed. We demonstrate that due to spin protection, these helical modes remain ballistic for large distances. Beyond the formation of helical modes, the new platform allows manipulations of quantum Hall edge modes which were not achievable so far and thus can serve as a rich playground for new research. Some new possibilities include artificial induction of compounded fractional edge modes and construction of new edge mode-based interferometers.

Acknowledgements

My Ph.D. work would not have been accomplished without the great people surrounding me and supporting me at the Weizmann Institute as well as in my personal life.

First, to Moty Heiblum. Since we met for the first time in your office, I knew I found my place. Your passion for great science is what makes the science you do so great. Your ability to motivate people to do great things is no less than shocking. Perhaps, some of it has to do with how much freedom you give your students to make mistakes and how much credit you give them when they succeed. In the seven years, I have been in your laboratory I always knew that I have all the support I could possibly need, whether it is actual resources, guidance, and mentoring, or just a listening ear. In those seven years, I had the freedom to peruse my own ideas and develop my own agenda as a scientist. You never forced any direction, methodology, or even a philosophy. And yet, I have learned everything there is to know about the research from you. Thank you.

To my research partner, Yuval Ronen, with whom I spent every day for the last 5 years. Besides learning from you and with you, and beyond struggling in research through difficult periods and succeeding together to finally produce physics we are proud of, I will always cherish the true partnership and deep friendship we had. You have made a huge impact on me which I will carry with me for the rest of my life.

To everyone in our research group. I can only wish for myself to be surrounded by, and work with, such incredible people, both professionally and personally. We can never take for granted the unique situation we have at the Weizmann Institute with regard to the quality of people around.

To Hadas Shtrikman for the best nanowires in the world, for her devotion and enthusiasm, and for treating every nanowire project as if it was her only one. To Valdimir Umansky for the world's best GaAs heterostructures, for his great intuition without which we could have never accomplished the project on which this thesis is about, and for his remarkable knowledge from which we can always learn.

To the submicron staff without whom the place would collapse. To Diana Mahalu, for her great care, for her readiness to assist us at all times, and for her

ability to dive into the smallest details which make our experiments possible and perfect them as no one else in the world can. To Olga Raslin, for endless efforts to help even on the expenses of her own time. To Yoram Rotblat who is a rare example of how one truly talented and experienced engineer could be better than ten mediocre ones and to Yossi Rolnik, for always helping, much more than expected. And to Vitaly Hanin, for his great help and support in our fabrication processes and for being a great office mate.

To my wife, Adi. When I started my M.Sc. in Moty's group, we just started dating. During our whole life together, I have been a researcher at the Weizmann Institute. Without your support and invaluable advice, I would have never made it through this journey.

Finally, to my parents, Doron and Ruti Cohen. Even the freedom I got from Moty during my research years is incomparable to the freedom I got from you throughout my entire life. And in a similar way, everything that I am is due to your unbelievable personality and your way of teaching me and reflecting to me what is truly important in life and what is not. You have always supported me in whatever I needed and provided me with the right tools and attitude which brought me to choose my track and do well in it.

Contents

Chapter 1
Introduction and Motivation: from Helical Modes to Topological Quantum Computing

1.1 Majorana Zero Modes and Topological Quantum Computing

1.1.1 Majorana Zero Modes

In recent years, great interest has been sparked in the condensed matter physics community due to the possibility of engineering exotic quantum states called *Majorana zero modes* (MZMs). These quasiparticles have remarkable exchange statistics, which makes them extremely interesting both from a fundamental physics point of view as well due to their potential to allow for protected quantum computations.

To understand what MZMs are and to describe their unique statistics, let's start with what we usually work with in condensed matter physics— electrons. Being fermions, electrons are described with the creation and annihilation operators, $c^\dagger$ and c, respectively, satisfying the anti-commutation relations:

$$\{c_i, c_j^\dagger\} = \delta_{ij}, \quad \{c_i, c_j\} = 0. \tag{1.1}$$

Operating with $c^\dagger$ on the ground state creates an electron above the Fermi energy and operating with c on the ground state removes an electron from below the Fermi energy (creating a hole).

Since the creation and annihilation operators, $c^\dagger$ and c, are complex, we can write them in terms of their real and imaginary components, called *Majoranan fermions* (MFs):

$$\begin{aligned} c &= \tfrac{1}{2}(\gamma_1 + i\gamma_2) \quad & c^\dagger &= \tfrac{1}{2}(\gamma_1 - i\gamma_2) \\ \gamma_1 &= c^\dagger + c & \gamma_2 &= i(c^\dagger - c). \end{aligned} \tag{1.2}$$

Y. Cohen, *A New Platform for Edge Mode Manipulations in the Quantum Hall Effect*, Springer Theses, https://doi.org/10.1007/978-3-030-05943-9_1

Evidently, MFs are their own anti-particles

$$\gamma = \gamma^{\dagger}, \tag{1.3}$$

and it also follows directly from the fermionic anti-commutation relations that the anti-commutation relations of MFs are:

$$\{\gamma_i, \gamma_j\} = 2\delta_{ij}. \tag{1.4}$$

MFs are named after Ettore Majorana who, in 1937, discovered real solutions to the Dirac equation, which by definition satisfy conditions (1.3) and (1.4) [1] [2]. But while these conditions make them exceptionally interesting in high energy and particle physics, in condensed matter physics this is not enough. In fact, every system of electrons could be written in terms of MFs, which by itself is merely a change of basis and does not lead to new physics (e.g. for each electron in a normal conductor we can write $c^{\dagger}c = \frac{i}{2}\gamma_1\gamma_2 + \frac{1}{2}$). MFs do become really interesting in condensed matter physics, however, when they commute with the Hamiltonian:

$$[\gamma_i, H] = 0. \tag{1.5}$$

Such a MF is called a MZM and the name ("zero mode") is adequate as commuting with the Hamiltonian implies that occupying the MZM leaves the system in the ground state:

$$H\gamma_i|g.s.\rangle = H|g.s.\rangle = E_{g.s.}|g.s.\rangle. \tag{1.6}$$

Most importantly, this condition also implies that the ground state is degenerate.

We will see later on how MZMs can actually be constructed in real systems, but first let's assume we have them and see why they are so interesting.

1.1.2 Topological Quantum Computing with Majorana Zero Modes

A system of $2N$ MZMs has a 2^N-fold degenerate ground state. This can be seen from the fact that each two MZMs form a single fermionic operator and the number operator, $c^{\dagger}c = \frac{i}{2}\gamma_1\gamma_2 + \frac{1}{2}$, can take two values, 0 and 1. Thus, there are 2^N basis states, $\{|\psi_1\rangle, |\psi_2\rangle, \ldots, |\psi_{2^N}\rangle\}$ and a specific ground state can be described as a linear combination:

[1] It is still debatable whether there are elementary particles in the universe which indeed satisfy these conditions (neutrinos are being investigated in this respect) [1].

$$|\psi\rangle = \sum_i a_i |\psi_i\rangle. \tag{1.7}$$

For example, a system with 4 MZMs has a 4-fold degeneracy with four basis states, $|00\rangle, |01\rangle, |10\rangle, |11\rangle$.

For a closed system, however, fermion parity must be conserved and therefore if the system is initialized in, say, an even parity state it will be limited to the two dimensional space spanned by $|00\rangle$ and $|11\rangle$ and the general state can be written as:

$$|\psi\rangle = \alpha|00\rangle + \beta|11\rangle. \tag{1.8}$$

This defines a qubit! Moreover, it can be shown [3, 4] that interchanging MZM i with MZM j results in a non-abelian unitary transformation in the subspace of ground states:

$$\begin{aligned} &|\psi\rangle \rightarrow U_{ij}|\psi\rangle \\ &U_{12}|00\rangle = \tfrac{1}{\sqrt{2}}(1+i)|00\rangle \\ &U_{23}|00\rangle = \tfrac{1}{\sqrt{2}}(|00\rangle + i|11\rangle) \\ &U_{34}|00\rangle = \tfrac{1}{\sqrt{2}}(1+i)|00\rangle\,. \end{aligned} \tag{1.9}$$

Note that these operations on the qubit only depend the topology of braiding MZMs, hence the name *topological quantum computation*. Finally, as we will see below, MZMs can be realized in systems where there is an energy gap above the ground state, which means that as long as perturbations are not too strong (weaker than the gap), the system will stay in the ground state. The only thing that can change the state of the system is braiding MZMs!

1.2 Forming Majorana Zero Modes in a Spinless p-Wave Superconductor

As discussed above, MZMs are superpositions of electrons and holes. It is therefore quite intuitive to look for them in superconductors (SCs), since the basic excitations in SCs, namely, the Boguliubov quasiparticles are also superpositions of electrons and holes. In the usual s-wave SC, however, the electron and hole making up a Boguliubov quasiparticle have opposite spins:

$$b = uc_{\uparrow}^{\dagger} + vc_{\downarrow} \tag{1.10}$$

Thus, even when $|u|^2$ and $|v|^2$ are equal–which in fact happens for q asiparticles that are just above the SC gap[2] as well as for sub-gap states that can actually be made to sit at zero energy [5]—the requirements for MZMs cannot be fulfilled. It follows that MZMs should be looked for in SCs with other types of pairing which form Cooper pairs in a triplet spin state leading to an effective spinless SC. While the first theoretical ideas for such systems where in exotic 2-dimensional systems with conjectured $p_x \pm ip_y$-wave pairing [6, 7], the simplest and most intuitive system is a 1-dimensional (1D) spinless p-wave SC. This system, which also proved to be most practical in recent experimental works, was first considered by Alexei Kitaev in 2001 [8]. To describe such a system and to demonstrate the emergence of MZMs, Kitaev considered a 1D tight binding model of N identical electronic sites with p-wave paring and no spin:

$$H = -\mu \sum_{i=1}^{N} c_i^\dagger c_i - \sum_{i=1}^{N-1} \left(t c_i^\dagger c_{i+1} + \Delta c_i c_{i+1} + h.c. \right) \tag{1.11}$$

Here μ is the chemical potential, c_i is the annihilation operator of an electron in site i, t is the hopping strength and Δ is the superconducting gap. Note that since there is no spin here, the superconducting term couples electrons on neighboring sites as a single site cannot be occupied by two electrons $(c_i^\dagger c_i^\dagger = 0)$.

As shown in Fig. 1.1, each electron can be broken into its MFs parts: $c_i = \frac{1}{2}(\gamma_{i,1} + i\gamma_{i,2})$. Then, for $\mu = 0$ and $\Delta = t$ the Hamiltonian reads,

$$H = -it \sum_{i=1}^{N-1} \gamma_{i,2}\gamma_{i+1,1}. \tag{1.12}$$

We can then construct new fermions made of two MFs on neighboring sites (Fig. 1.1)—$a_i = \frac{1}{2}(\gamma_{i+1,1} + i\gamma_{i,2})$. Amazingly enough, writing the Hamiltonian again in terms of the new fermions, we get a diagonalized Hamiltonian,

$$H = 2t \sum_{i=1}^{N-1} a_i^\dagger a_i. \tag{1.13}$$

So far this seems merely as mathematical way of diagonalizing the Hamiltonian. The final eigenstates are the usual fermionic states with a finite excitation energy. However, looking more closely at the Hamiltonian (1.12), we observe that the two

[2]Solving the Bogoliubov-deGenes equations one finds $|u(\varepsilon)|^2 = \frac{1}{2}\left[1 + \frac{\sqrt{\varepsilon^2 - \Delta^2}}{\varepsilon}\right]$ and $|v(\varepsilon)|^2 = \frac{1}{2}\left[1 - \frac{\sqrt{\varepsilon^2 - \Delta^2}}{\varepsilon}\right]$

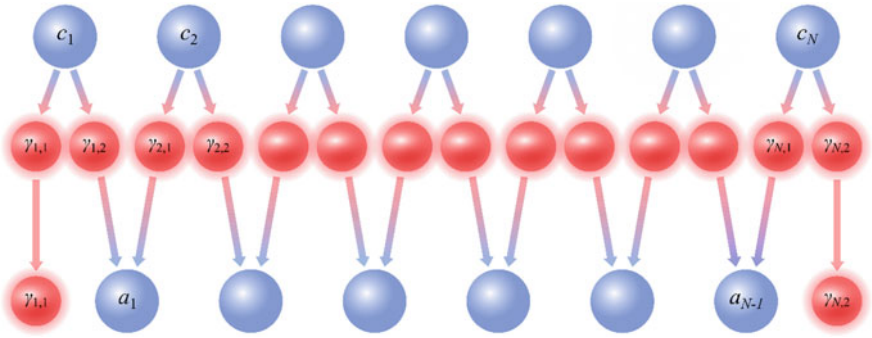

Fig. 1.1 Kitaev's chain. The blue spheres denote fermionic states while the red spheres denote MFs. For $\mu = 0$ and $\Delta = t$ the Hamiltonian is diagonalized by a set of fermionic states each made of a pair of MFs from neighboring sites, while two MZMs remain unpaired at the ends

MFs at the ends of the chain, $\gamma_{1,1}$ and $\gamma_{N,2}$, are completely absent! Thus, they evidently commute with the Hamiltonian and we get MZMs.

Note that, as mentioned above, the MZMs are accompanied by an energy gap, $2t$, which is important to allows for topologically protected operations. Also, while we described the scenario for the very unique "sweet spot" where $\mu = 0$ and $\Delta = t$, it can be shown that the MZMs survive as long as the chemical potential is inside the gap, $|\mu| < 2t$ [8]. If the chemical potential is not zero, however, the MZMs get delocalized with an exponential decay into the bulk of the chain. In this case, the fermionic state made from them, $f = \frac{1}{2}(\gamma_{1,1} + i\gamma_{N,2})$, develops a finite energy which is exponentially small in the length of the chain.

The essential physics of the Kitaev model can be generalized to a continuous version of a 1D p-wave SC as well as a 2D $p_x \pm ip_y$-wave SC. In the 1D case MZMs can again be obtained at the ends of a long wire [9–11], while in the 2D case MZMs will appear in vortices of the SC [3, 12].

1.3 Forming a Spinless p-Wave Superconductor from Helical Modes

It is because of its simplicity and elegancy that the Kitaev chain "rubs the salt on the womb"—where can we find a system with such exotic p-wave superconducting pairing? As mentioned above, some exotic systems, such as the fractional quantum Hall state $\nu = 5/2$ [6] and such as Sr2RuO4 [7], have been proposed to exhibit $p_x \pm ip_y$-wave pairing and in fact, several experimental works, strongly support the existence of MZMs in the former [13–16]. However, the experimental control over these systems is extremely difficult, making future research possibilities very limited, let alone practical manipulations of MZMs.

Fortunately, another approach can be taken. In 2008 Fu and Kane realized that it is possible to create an effective spinless SC by inducing *s*-wave superconductivity on the surface of a topological insulator (TI) [17]. While their proposal was for the 2D surface of a 3D TI, it works in a similar way for the 1D edge of a 2D TI and this 1D version is easier to relate to our above discussion of a 1D spinless *p*-wave SC. Moreover, the most successful experimental works of recent years were based on systems that resemble the 1D version of Fu and Kane's proposal.

The 1D edge of a 2D TI carries a unique edge mode structure: two 1D edge modes with opposite spins counter-propagate against each other (Fig. 1.2a). Such modes are called *helical modes*. The name comes from the fact that the spin is locked with the direction of motion, making the helicity a well-defined quantum number. Note that in a system with no coupling between opposite spins the helical modes will not mix and transport of electrons on the edge modes will be protected from backscattering. Most importantly, coupling the helical modes to a conventional *s*-wave SC, thus inducing the usual SC pairing $\Delta c_{k\uparrow} c_{-k\downarrow}$, creates an effective spinless *p*-wave SC!

An intuitive way to understand the effective *p*-wave pairing is to note that a spin singlet cannot be made from the electronic states of the helical modes, because there is no spin degeneracy (each *k*-state has a specific spin). At the same time, there are

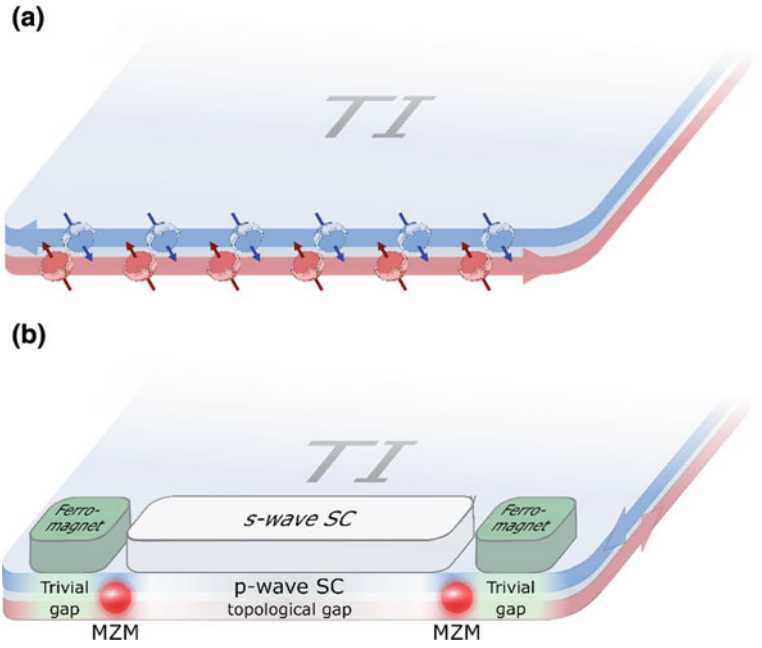

Fig. 1.2 **a** Helical modes at the edge of a topological insulator. **b** When a conventional s-wave SC is coupled to the helical modes, a p-wave SC emerges. If trivial gaps are opened near the ends of the SC region, for example by coupling ferro-magnets to the helical modes, localized Majorana zero modes emerge

states in the system with opposite spins and momentum so that SC pairing can still take place via the pairing term $\Delta c_{k\uparrow} c_{-k\downarrow}$. The helical modes system together with induced superconductivity from an *s*-wave SC is described by the Hamiltonian,

$$H = \int \left[\sum_{\sigma} c_{\sigma}^{\dagger} (-i v_F \sigma \partial_x - \mu) c_{\sigma} + (\Delta c_{\uparrow} c_{\downarrow} + h.c.) \right] dx, \tag{1.14}$$

with $\sigma = 0, 1 = \uparrow, \downarrow$ the spin, v_F the Fermi velocity, μ the chemical potential and Δ the induced SC pairing. In *k*-space this is

$$H = \sum_{k} \left[\sum_{\sigma} (v_F k \sigma - \mu) c_{k\sigma}^{\dagger} c_{k\sigma} + (\Delta c_{k\uparrow} c_{-k\downarrow} + h.c.) \right]. \tag{1.15}$$

As done in ref. 18 [18], to see how this gives effective *p*-wave pairing, motivated by the well-defined helicity in the system we define new operators:

$$\begin{aligned} u_k &= \begin{cases} c_{k\uparrow} & \text{for} \quad k > 0 \\ c_{k\downarrow} & \text{for} \quad k < 0 \end{cases} \quad \text{helicity} + 1 \\ d_k &= \begin{cases} c_{k\uparrow} & \text{for} \quad k < 0 \\ c_{k\downarrow} & \text{for} \quad k > 0 \end{cases} \quad \text{helicity} - 1. \end{aligned} \tag{1.16}$$

The Hamiltonian then becomes:

$$H = \sum_{k} \left[-(\mu - v_F |k|) u_k^{\dagger} u_k - (\mu + v_F |k|) d_k^{\dagger} d_k + \left(\frac{\Delta \text{sgn} k}{2} (u_k u_{-k} + d_k d_{-k}) + h.c. \right) \right], \tag{1.17}$$

with sgn the sign function. This Hamiltonian describes two independent species with *p*-wave pairing! Moreover, the *u* states fill up all positive energies while the *d* states fill up all negative energies. Therefore, μ will always be located in the energy band of one and only one specie leading to an effective spinless *p*-wave SC.

Finally, an important note should be made on the requirement for MZMs formation. Since the above discussion described the edge modes of a 2D TI, the MZMs at the ends of the induced superconducting region of the edge will not be localized and instead will be smeared on the entire non-superconducting region of the edge. In fact, this will cause the MZMs to couple and hybridize. To avoid this and localize the MZMs, it is necessary to introduce a coupling between the two spins in the non-superconducting region of the edge which will open a gap (a non-topological gap). This could be done for example by coupling the edge modes to ferromagnets as shown in Fig. 1.2b. As described below (Sect. 1.5), there are also 1D schemes in which this issue is not present.

1.4 Parafermions and Fractional Helical Modes

1.4.1 Parafermions, Fibonacci Fermions and Universal Topological Quantum Computing

While MZMs can define qubits as discussed above, the set of topologically protected operations that can be performed on such qubits braiding MZMs is limited. In fact, from the unitary transformation (1.9) it can be seen that for a qubit defined from four MZMs, braiding operations can only explore the six poles of the Bloch sphere. However, there is a generalization of MZMs, called parafermionic zero modes (PFZMs), which can do better.

Parafermions (PFs) are a generalization of MFs and are defined by the operators α_j satisfying

$$(\alpha_j)^d = 1, \quad \alpha_j\alpha_k = e^{2\pi i \mathrm{sgn}(k-j)/d}\alpha_j\alpha_k, \quad d \text{ is some integer} \tag{1.18}$$

It is easy to verify that for $d = 2$ this condition reduces to the condition for MFs. When two PFs, α and β, are unpaired and absent from the Hamiltonian in a similar way to the MFs in the Kitaev chain, they commute with the Hamiltonian and form PFZMs. The operator $\alpha^\dagger\beta$ creates d distinct eigenstates (from (1.18) it can be seen that there are d different eigenvalues), and therefore a pair of PFZMs give rise to a d-fold ground state degeneracy.

This generalization allows for much richer and more useful topologically protected braiding operations on qubits defined from PFZMs [19]. Moreover, while these PFZMs are still not quite enough for universal quantum computing, they can be used to engineer yet other entities called *Fibonacci anyons* [20], the braiding of which gives a universal set of gates. While we will not describe Fibonacci anyons here, they are clearly a holy grail for topological quantum computing and they give a strong motivation for constructing PFZMs.

1.4.2 Forming Parafermionic Zero Modes in Fractional Helical Modes

The general PFs are much harder to find than MFs. As described above, two MFs form a usual fermionic operator and hence, MFs are present almost everywhere and we only need to think of a clever way to unpair them to form MZMs. On the other hand, the very unusual commutation relations of (1.17) makes searching for PFs more difficult. Fortunately, there is a system that provides exactly what is needed: the fractional quantum Hall effect system.

We will discuss both the integer quantum Hall effect (IQHE) and the fractional quantum Hall effect (FQHE) in greater detail in the next chapter, however, for now

we only mention that a 2D system in the quantum Hall regime harbors 1D edge modes. Remarkably, while the edge modes of the IQHE carry electrons, those of the FQHE carry anyonic excitations which obey very similar relations to (1.17)! In a similar way to the formation of MZMs, when two counter-propagating edge modes of the FQHE with opposite spins are coupled to a conventional SC, PFZMs form at the ends of the induced SC region [21]. As we shall see later, forming these so called *fractional helical modes* is a major challenge, which we overcome in this work.

1.5 Previous Experimental Work—Successes and Challanges

In the past decade, significant experimental efforts were made to demonstrate the emergence of helical modes in several systems as well as to induce superconductivity in those systems. We now discuss briefly the main investigated platforms, the main experimental achievements that were made, and the main challenges of each platform.

1.5.1 Edge States of Topological Insulator

In 2007, following a theoretical proposal suggesting that HgTe quantum wells can become TI [22], Konig et al. have demonstrated for the first time the emergence of helical modes. A couple of years later, Knez et al. showed similar results in InAs/GaSb quantum wells [23]. In addition, superconductivity was successfully induced in the HgTe and some evidence for topological superconductivity was observed [24–26].

While these systems are evidently very promising and efforts are being made to form and probe MZMs in them, important challenges remain. First, the helical modes where observed only for a relatively small system size on the order of 1–5 microns. In addition, these materials are difficult to work with and new methods must be developed to allow fabrication of complicated device structures which will lead to MZMs formation and manipulation. Finally, there is no known rout towards forming the more general PFZMs in these systems. Although there are some theoretical works exploring possible emergence of PFZMs in these systems [27–29], they all require fine-tuning of parameters, and moreover, arrive at PFZMs that are in fact not topologically protected.

1.5.2 Semiconducting Nanowires with Strong Spin-Orbit Interaction

In 2010, two important theoretical works [9, 10] proposed that a semiconducting nanowire with strong spin-orbit coupling and large Lande g-factor can exhibit

(approximately) helical modes in the presence of an external magnetic field. Then, when such a nanowire is coupled to a SC contact, the portion of the NW which is coupled to the SC is expected to become a topological SC with MZMs at the ends. Following these proposals, a few experimental groups developed such nanowire-SC hybrid devices and in 2012 observed the first evidence for MZMs: a zero bias peak in the differential conductance measured by tunneling spectroscopy to the end of the device.

Since these discoveries, significant resources and efforts were invested in further developing the nanowire-SC platform and evidence for MZMs continued to accumulate. However, there are several important challenges to this platform. First, there are still competing theoretical explanation for the zero bias peak and a "smoking gun" for the MZMs emergence is still missing. Second, the emergence of helical modes in these semiconducting nanowires was never convincingly observed and in fact, even the 1D nature of the band structure is difficult to confirm in a reproducible way. Since the electrons in the nanowire are very sensitive to the disorder on its surface, in many cases the transport behavior points towards a 0D behavior (a quantum dot, or a series of quantum dots instead of a continuous 1D band). The sensitivity to disorder also leads to a limitation on the size of the devices that can be made which in turn might limit the protection of the MZMs. Third, semiconducting nanowires are difficult to work with in terms of device fabrication, and scaling up these systems for real quantum computing applications seems extremely challenging at the current stage. Finally, just as for the TI's edge states platform, there is no known way to form protected PFZMs with these 1D systems.

1.5.3 Graphene

Given some of the challenges described above, it is not surprising that other platforms are being investigated for the formation of helical modes and fractional helical modes. Perhaps the most famous system that exhibits robust ballistic 1D edge mode transport is the quantum Hall effect system. Moreover, as mentioned above, the FQHE offers a clear theoretical rout for the creation of PFZMs. Recently successful engineering of helical edge modes was reported in twisted bilayer graphene in the IQHE regime [30]. This system does not suffer from many of the problems discussed above and seems to have very promising prospects. In fact, it is close in nature to the platform developed in our work on double quantum wells of GaAs heterostructures. While the graphene system has an advantage of easy coupling to a SC, the GaAs system has very robust FQHE states, has mature and well developed methods of MBE growth and fabrication that allow a variety of device architectures with a high tunability of parameters (*e.g.* the coupling between counter-propagating modes, which can be extremely important for topological phases to be formed), and is highly reproducible and scalable. Moreover, recent works successfully coupled such GaAs systems to SC contacts [31].

1.6 Summary

MZMs in condensed matter systems are extremely interesting both due to their fascinating physical properties as well as due to their predicted usefulness for topologically protected quantum computation and quantum information applications. The most promising way to form MZMs, which has had some important success in recent years, is via inducing superconductivity by an *s*-wave SC in a system with helical modes. While numerous experimental works have had success in demonstrating helical modes and some evidence for MZMs are accumulating, each experimental platform has its own challenges, some in the robustness of the effects, some in reproducibility, and some in scalability that is needed to form complicated electronic devices for future research and applications. Moreover, no experimental platform have demonstrated fractional helical modes.

Below, we introduce the new platform we developed for integer and fractional QHE edge mode manipulations. This platform is based on the well-known GaAs/AlGaAs heterostructure system, which is extremely clean, robust, easy to work with and scalable. Using this platform we demonstrated the formation of robust helical modes and, for the first time to the best of our knowledge, the formation of fractional helical modes. Moreover, the platform can be used for a variety of new experiments with quantum Hall edge modes as will be discussed.

References

1. Wilczek, F.: Majorana returns. Nat. Phys. **5**, 614–618 (2009)
2. Majorana, E.: Teoria simmetrica dell'elettrone e del positrone. Nuovo. Cim. **14**, 171–184 (1937)
3. Ivanov, D.A.: Non-Abelian statistics of half-quantum vortices in p-wave superconductors. Phys. Rev. Lett. **86**, 268–271 (2001)
4. Alicea, J., Oreg, Y., Refael, G., von Oppen, F., Fisher, M.P.A.: Non-Abelian statistics and topological quantum information processing in 1D wire networks. Nat. Phys. **7**, 412–417 (2011)
5. Lee, E.J.H., et al.: Spin-resolved Andreev levels and parity crossings in hybrid superconductor–semiconductor nanostructures. Nat. Nanotechnol. **9**, 79–84 (2014)
6. Moore, G., Read, N.: Nonabelions in the fractional quantum Hall effect. Nucl. Phys. B **360**, 362–396 (1991)
7. Das Sarma, S., Nayak, C., Tewari, S.: Proposal to stabilize and detect half-quantum vortices in strontium ruthenate thin films: non-Abelian braiding statistics of vortices in a px + ipy superconductor. Phys. Rev. B **73**, 220502 (2006)
8. Kitaev, A.Y.: Unpaired Majorana fermions in quantum wires. Phys. Usp. **44**, 131–136 (2001)
9. Lutchyn, R.M., Sau, J.D., Das Sarma, S.: Majorana fermions and a topological phase transition in semiconductor-superconductor heterostructures. Phys. Rev. Lett. **105**, 77001 (2010)
10. Oreg, Y., Refael, G., Von Oppen, F.: Helical liquids and Majorana bound states in quantum wires. Phys. Rev. Lett. **105**, 177002 (2010)
11. Nilsson, J., Akhmerov, A.R., Beenakker, C.W.J.: Splitting of a Cooper Pair by a pair of Majorana bound states. Phys. Rev. Lett. **101**, 120403 (2008)

12. Read, N., Green, D.: Paired states of fermions in two dimensions with breaking of parity and time-reversal symmetries and the fractional quantum Hall effect. Phys. Rev. B **61**, 10267–10297 (2000)
13. Dolev, M., Heiblum, M., Umansky, V., Stern, A., Mahalu, D.: Observation of a quarter of an electron charge at the ν = 5/2 quantum Hall state. Nature **452**, 829–834 (2008)
14. Bid, A., et al.: Observation of neutral modes in the fractional quantum Hall effect regime. In AIP Conference Proceedings, **1399,** 633–634 (2011)
15. Willett, R.L., Pfeiffer, L.N., West, K.W.: Measurement of filling factor 5/2 quasiparticle interference with observation of charge e/4 and e/2 period oscillations. Proc. Natl. Acad. Sci. U. S. A. **106**, 8853–8858 (2009)
16. Banerjee, M., et al.: Observation of half-integer thermal Hall conductance arXiv:1710.00492 (2017)
17. Fu, L., Kane, C.L.: Superconducting proximity effect and Majorana fermions at the surface of a topological insulator. Phys. Rev. Lett. **100**, 96407 (2008)
18. Potter, A.C., Lee, P.A.: Engineering a p+ ip superconductor: comparison of topological insulator and Rashba spin-orbit-coupled materials. Phys. Rev. B **83** (2011)
19. Hutter, A., Loss, D.: Quantum computing with parafermions. Phys. Rev. B **93**, 125105 (2016)
20. Alicea, J., Fendley, P.: Topological phases with parafermions: theory and blueprints. Annu. Rev. Condens. Matter Phys. **7**, 119–139 (2016)
21. Clarke, D.J., Alicea, J., Shtengel, K.: Exotic non-abelian anyons from conventional fractional quantum Hall states. Nat. Commun. **4**, 1348 (2013)
22. Bernevig, B.A., Hughes, T.L., Zhang, S.-C.: Quantum spin hall effect and topological phase transition in HgTe quantum wells. Science **314**, 1757–1761 (2006)
23. Knez, I., Du, R.-R., Sullivan, G.: Evidence for helical edge modes in inverted InAs/ GaSb quantum wells. Phys. Rev. Lett. **107**, 136603 (2011)
24. Bocquillon, E., et al.: Gapless Andreev bound states in the quantum spin Hall insulator HgTe. Nat. Nanotechnol. **12**, 137–143 (2016)
25. Hart, S., et al.: Induced superconductivity in the quantum spin Hall edge. Nat. Phys. **10**, 638–643 (2014)
26. Deacon, R.S., et al.: Josephson radiation from gapless Andreev bound states in HgTe-based topological junctions. Phys. Rev. X **7**, 21011 (2017)
27. Oreg, Y., Sela, E., Stern, A.: Fractional helical liquids in quantum wires. Phys. Rev. B **89**, 115402 (2014)
28. Klinovaja, J., Loss, D.: Time-reversal invariant parafermions in interacting Rashba nanowires. Phys. Rev. B **90**, 45118 (2014)
29. Klinovaja, J., Loss, D.: Parafermions in an interacting nanowire bundle. Phys. Rev. Lett. **112**, 246403 (2014)
30. Sanchez-Yamagishi, J.D., et al.: Helical edge states and fractional quantum Hall effect in a graphene electron–hole bilayer. Nat. Nanotechnol. **12**, 118–122 (2016)
31. Wan, Z., et al.: Induced superconductivity in high-mobility two-dimensional electron gas in gallium arsenide heterostructures. Nat. Commun. **6**, 7426 (2015)

Chapter 2
The Quantum Hall Effect

2.1 Two-Dimensional Electron Gas System in GaAs Heterostructures

In the last four decades, one of the most ubiquitous and fruitful platforms for condensed matter physics experiments was the 2D electron gas (2DEG) system embedded in GaAs/AlGaAs heterostructures. Such heterosrtuctures and the use of modulation doping leads to a system of electrons that are free to move with incredible high mobility in the *x*-*y* plane while they have no motion in the z-direction.

GaAs and AlAs have an extremely good lattice matching (lattice mismatch of $\sim$0.1%). Therefore, an almost perfect heterostructure of $Al_xGa_{1-x}As$/GaAs, with any alloy composition (any *x*) and any layer thickness can be grown with no dislocations near the interface. Such heterostructures can be grown by molecular beam epitaxy (MBE), which allows extremely high precision in layer thickness, alloy composition, doping concentration and most importantly, extremely clean crystals with very low impurities concentrations.

Since GaAs and $Al_xGa_{1-x}As$ have different band gaps (for GaAs $\sim$1.4 eV and for $Al_{0.35}Ga_{0.65}As$ $\sim$2.0 eV), the band structure can be engineered in various ways. Two methods to form a 2DEG are typically used as shown in Fig. 2.1. In Fig. 2.1a a single GaAs/AlGaAs interface is used to create a sharp drop in the bottom of the conduction band. When silicon donors are added in the AlGaAs layer some distance from the interface, electrons from the donors migrate to the interface and create a band banding as shown in Fig. 2.1c. This leads to a "triangular" potential well next to the interface, which confines the electrons (Fig. 2.1e). In typical samples, the electron density is tuned such that only the first electronic subband in the well is occupied, leading to no degree of freedom along the *z*-direction and therefore an effective 2D behavior; hence the name 2DEG. Since the GaAs/AlGaAs interface is very smooth, and since the donors layer is far away from the 2DEG, the mobility can be incredibly high (above 20×10^6 cm^2/V-s in some realizations [1]).

Y. Cohen, *A New Platform for Edge Mode Manipulations in the Quantum Hall Effect*, Springer Theses, https://doi.org/10.1007/978-3-030-05943-9_2

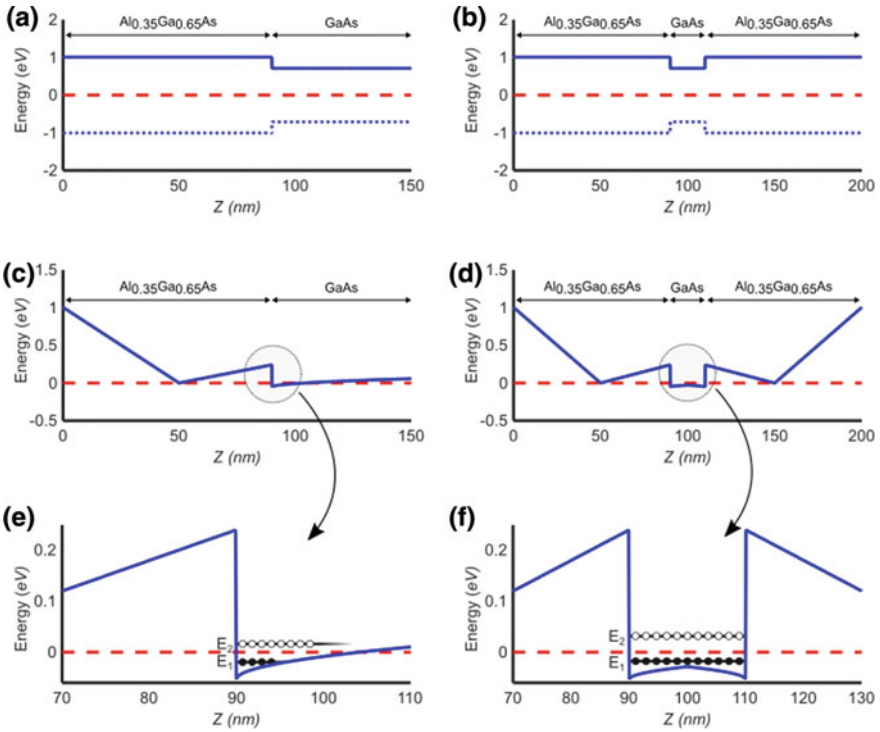

Fig. 2.1 Forming a 2DEG GaAs/AlGaAs heterostructures. **a** A single GaAs/AlGaAs interface creates a sharp drop in the bottom of the conduction band. When silicon donors are added in the AlGaAs layer some distance from the interface, electrons from the donors migrate to the interface and create a band banding **c**, which in turn leads to a "triangular" potential well that confines the electrons next to the interface **e**. **b** A GaAs layer sandwiched between two layers of AlGaAs, creating a potential well in the conduction band. Double side doping can be used **d**, which leads to greater flexibility in the quantum well design and in the charge density in the well. It also allows for a significantly higher mobility

The second method to form a 2DEG is to sandwich a GaAs layer between two layers of AlGaAs. In this so called *quantum well* method[1], the bottom of the conduction band forms a potential well, as shown in Fig. 2.1b. The size of the well can be chosen in the MBE growth and doping can be introduced in both sides of the well (Fig. 2.1d). This leads to a greater flexibility in the subbands' wave functions as well as in their energy separation. Moreover, due to the double side doping an even higher mobility, of as high as 36×10^6 cm^2/V-s, can be achieve [1].

[1]The first method of a single interface is simply referred to as GaAs/AlGaAs 2DEG while the second method of GaAs sandwitched between two AlGaAs regions is referred to as a quantum well heterostructure.

The high mobility and the richness of the fabrication methods, which where developed for these structures, allowed for complicated devices to be constructed and for a great deal of physics to be investigated. A non-exhaustive list includes: electron coherence and interference, quantum dots physics, Kondo physics, spin qubits, quantum Hall effect, fractional quantum Hall effect, neutral modes and quantization of thermal conductance. Here, we focus on the integer and fractional quantum Hall effects, which lead to robust 1D edge modes that we will utilized to create helical modes.

2.2 Classical Hall Effect

In 1879 Edwin Hall discovered the famous Hall Effect [2] and opened the way to more than a 100 years of new physics. The basic measurement, called a Hall measurement, is described in Fig. 2.2 When current, I_x, flows in the x-direction through a rectangular 2DEG (or even just a thin rectangular conductor), called a Hall bar, which is subject to a perpendicular magnetic field, B, in the z-direction, a voltage, V_y, develops in the y-direction. In addition to this so called Hall voltage, and as usual, a voltage V_x develops in the direction of the current. We define the transverse and longitudinal resistances as follows

$$\begin{aligned} R_{xy} &= \frac{V_y}{I_x} \\ R_{xx} &= \frac{V_x}{I_x} \end{aligned} \tag{2.1}$$

While the longitudinal resistance is independent of B, the transverse resistance is linear in B (Fig. 2.2b). The Drude model, which describes the electrons as non-interacting point like particles that collide with impurities at an average rate of $1/\tau$, describes the physics of the classical Hall Effect well. In this model the electrons move according to the equation,

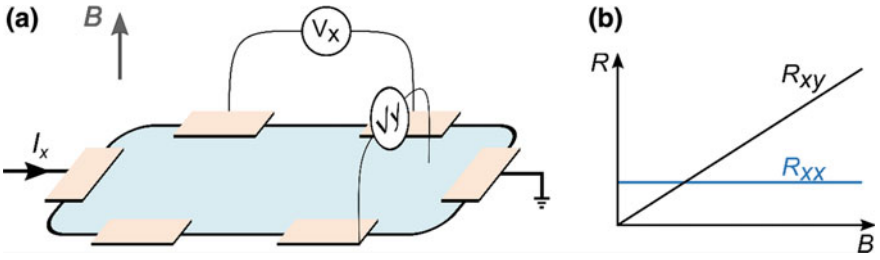

Fig. 2.2 Hall measurement

$$\frac{d\vec{p}}{dt} = -\frac{\vec{p}(t)}{\tau} + \vec{f}(t), \tag{2.2}$$

with $\vec{p}(t)$ the momentum of the electron at time t, and $f(t)$ the force on the electron at time t. Plugging in the force from the electric field, $e\vec{E}$, and the Lorentz force from the magnetic field, $e\vec{v} \times \vec{B}$, and remembering that $\vec{I} = en\vec{v} = en\vec{p}/m$ gives at steady state $\frac{d\vec{p}}{dt} = 0$:

$$\begin{pmatrix} \frac{m}{e^2 n\tau} & \frac{B}{en} \\ -\frac{B}{en} & \frac{m}{e^2 n\tau} \end{pmatrix} \begin{pmatrix} I_x \\ I_y \end{pmatrix} = \begin{pmatrix} E_x \\ E_y \end{pmatrix} \longrightarrow \begin{matrix} R_{xy} = \frac{B}{ne} \\ R_{xx} = \frac{1}{en\mu} \end{matrix} \tag{2.3}$$

With $\mu = e\tau/m$ the mobility of the electrons in the system, e and m the electron's charge and mass, respectively, and n the charge density. Thus, from the simple classical Hall measurement we can obtain the charge carriers' density, the sign of their charge, and the mobility.

2.3 Integer Quantum Hall Effect

In 1980 Klaus von Klitzing discovered a new behavior of the Hall effect that emerges when a 2DEG is cooled down to sufficiently low temperatures [3]. At certain ranges of magnetic field, the Hall resistance deviates from the classical prediction and exhibits plateaus at perfectly quantized values of resistance, which correspond to integer numbers of the conductance quanta:

$$R_{xy} = \frac{1}{i}\frac{h}{e^2} \quad (i \text{ integer}) \tag{2.4}$$

Moreover, the resistance plateaus are accompanied by a vanishing longitudinal resistance,

$$R_{xx} = 0 \tag{2.5}$$

This effect, which is demonstrated in Fig. 2.3, is called the integer quantum Hall effect (IQHE). In 1985 Von Klitzing won the Nobel for its discovery.

2.3.1 Landau Levels

The IQHE is a result of the quantization of the energy of electrons in 2D that are subject to a perpendicular magnetic field. In the absence of magnetic field, the electrons in the 2DEG fill up a Fermi see with a constant density of states

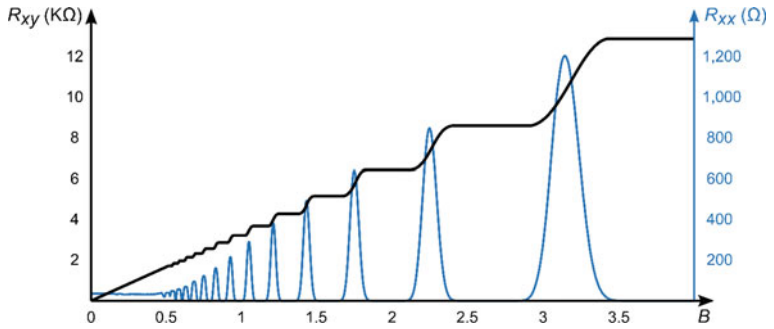

Fig. 2.3 Integer quantum Hall effect

(2D dos = $\frac{m*}{\pi\hbar^2}$). However, the addition of a perpendicular magnetic field, B, quantizes the spectrum into a series of discrete and degenerate energy levels, called Landau levels (LLs), with energies

$$E_n = \hbar\omega_c(\frac{1}{2} + n) \tag{2.6}$$

where $\omega_c = \frac{eB}{m^*}$ is the cyclotron frequency.

Each LL further spin-split due to the Zeeman energy, $E_Z = g * \mu_B B$. Figure 2.4, shows the energy levels as a function of B, a diagram called a fan diagram. For simplicity of notation, we will refer to the final spin-split energy levels simply as LLs. Then, as shown in Fig. 2.4, the odd LLs (L1, LL3, etc.) are separated by $\hbar\omega_c$, while each even LL (LL2, LL4, etc.) lies $2g * \mu_B B$ above the previous odd LL.

Each (spin-split) LL has a degeneracy of $g = \frac{B}{\phi_0}$ per unit area, with $\varphi_0 = \frac{h}{e}$ the magnetic flux quantum. This means that for every unit area, the number of states in

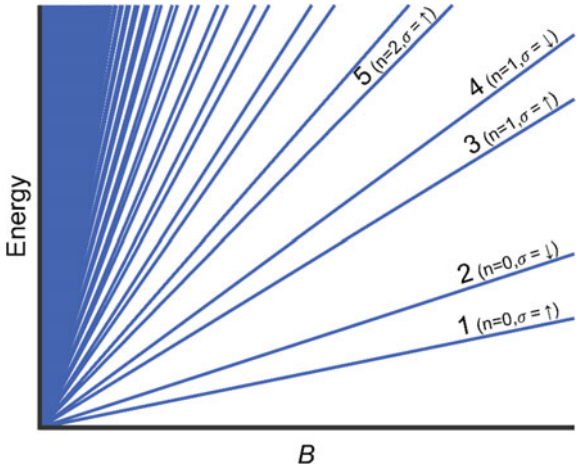

Fig. 2.4 Fan diagram. The energies of the Landau levels as a function of magnetic field

each LL equals the number of flux quanta penetrating through the area. The number of filled LLs is called the filling factor and is denoted by ν. For a fixed electron density n, we therefore get,

$$\nu = \frac{n}{g} = \frac{nh}{eB} \tag{2.7}$$

The eigenstates of the system can be written (in a particular choice of gauge) as,

$$\psi_{n,k_x}(x,y) = \frac{1}{\sqrt{L}} e^{ik_x x} \chi_{n,k_x}(y) \tag{2.8}$$

with $\chi_{n,k_x}(y)$ the wave function of an harmonic oscillator centered at $y = y_{k_x} = \frac{\hbar k_x}{eB}$.

Thus, we see that the electrons are free propagating waves in the x-direction, while they are localized in the y-direction, with each electron localized around a position proportional to ${k_x}^2$. And since the LLs are flat in k-space, they are flat in position space. However, this picture does not take the confining potential nor the disorder potential into account. Let's add them now one by one.

2.3.2 *Confining Potential*

The energies of the LLs approximately follow the confining potential and bend upwards towards the edge as shown in Fig. 2.5. Therefore, each filled LL intersects the Fermi energy at the edge in a single point in space, creating 1D edge mode. A straight forward calculation shows that each edge mode has a conductance quantum of $\frac{e^2}{h}$. Moreover, the current carried by this state is chiral, *i.e.* it flows around the edge of the sample either clockwise or counter-clockwise depending on the direction of B. A good intuition for this can be obtained from noticing that the velocity of the electrons along the edge is proportional to the slope of the energy w. r. t the wave vector, which in turn is proportional to the slope of the energy w.r.t position (*e.g.* in the Landau gauge above $\frac{d\varepsilon}{dk} = \frac{\hbar}{eB}\frac{d\varepsilon}{dy}$). Since the LL always bends upwards towards the edge, the velocity is always chiral, with the direction (clockwise or counter-clockwise) given by the direction of B.

We see now that if the filling factor, ν, in the bulk is an integer, there are ν chiral edge modes and therefore the conductance along the edge is,

[2]Note that these eigenstates are a result of a specific choice of gauge for the vector potential. Other gauge choices would lead to other results such as switching the roles of x and y (this is obvious as there is complete symmetry between x and y in our discussion so far), but this would not lead to any difference in our discussion

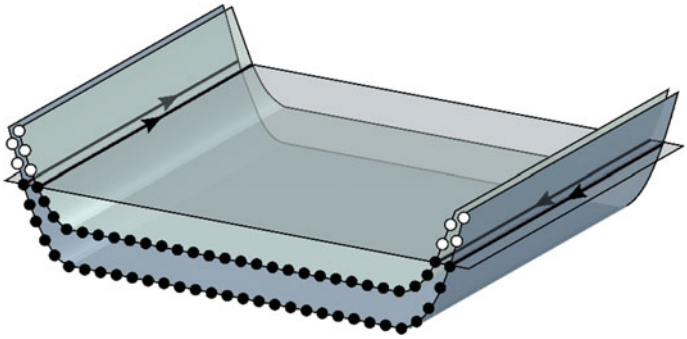

Fig. 2.5 Landau levels in a confining potential. Since the Landau levels follow the confining potential, they bend towards the edges, which leads to the formation of 1D chiral edge modes

$$\sigma = \frac{e^2}{h} v \tag{2.9}$$

When current is injected at the source contact of a Hall bar, since the bulk is gapped and since the current flowing on the edge is chiral, all the current reaches the ground contact (Fig. 2.6). The potential along the edge is therefore constant all the way from the source contact to the ground contact (red edge modes in Fig. 2.6), and is equal to:

$$V_{\text{hotedge}} = I_x \sigma = I_x \frac{e^2}{h} v \tag{2.10}$$

The potential along the edge leaving the ground contact and going to the source contact (blue edge in Fig. 2.6) is also constant and equal to the ground potential,

$$V_{\text{coldedge}} = 0 \tag{2.11}$$

This gives the correct Hall resistance as well as the vanishing longitudinal resistance only for integer filling factors! It still does not explain the plateaus. For this, we must to add disorder.

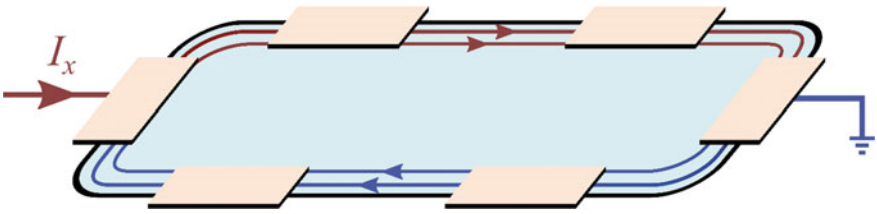

Fig. 2.6 Current injected to quantum Hall edge modes

2.3.3 *Disorder Potential*

In a similar way to the LLs following the edge potential, we can imagine that they follow the hills and valleys of the disorder potential. As shown in Fig. 2.7. This leads to a classification of the bulk states to two kind of states:

Localized states: states that become localized around the disorder potential's hills and valleys. Due to the localization, the energies of these states are shifted from the LL energy which leads to broadening of the LLs (Fig. 2.7a, c).

Extended states: states that lie on the zero potential, equipotential lines in the disorder landscape. The energy of these states is therefore always in the center of the LL (Fig. 2.7b).

Note that, very importantly, the disorder does not change significantly the behavior on the edge. For each energy above the center of the LL energy, there will be an extended state laying on an equipotential line a on the edge. The only thing that the disorder does is to make this state go in some more complicated "zig-zags" around the disorder's hills and valleys.

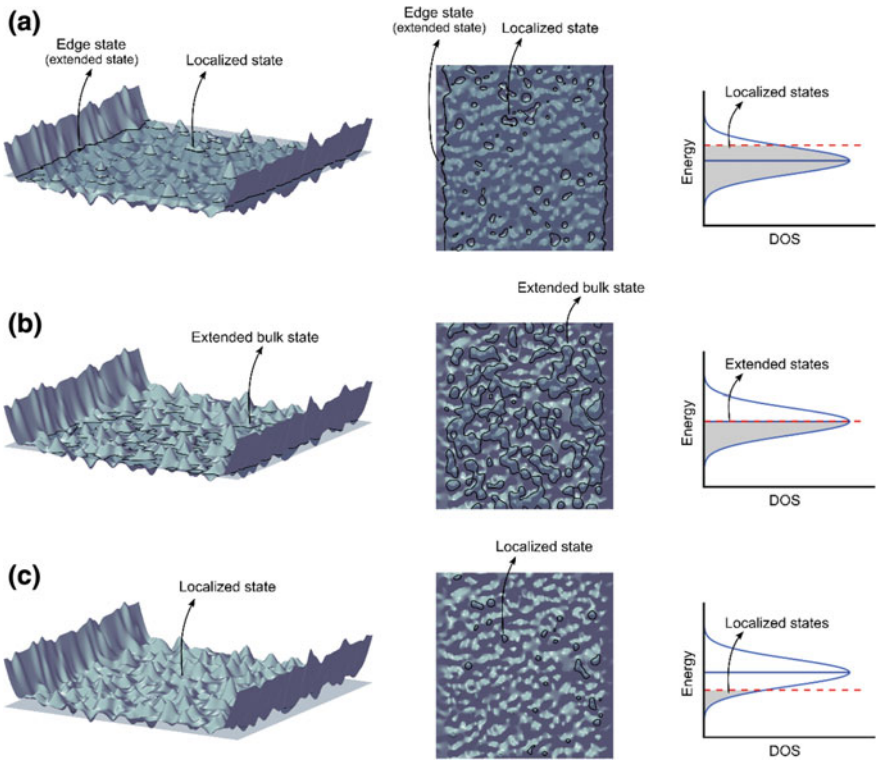

Fig. 2.7 LLs broadening in a disorder potential & localized and extended states

This now explains the plateaus. As can be seen in Fig. 2.7, the LLs broadening helps fixing the Fermi energy in between the centers of two LLs, for a range of filling factors around integer fillings. Even when the filling factor is not a perfect integer, the Fermi energy lies between the centers of two LLs, and while it is in the range of the localized bulk states, the bulk is still insulating (in a *mobility gap*). Moreover, since the Fermi energy is above the center of an integer number of LLs, there is an integer number of edge modes and the conductance on the edge is quantized.

The result is that for a range of magnetic fields, corresponding to a range of filling factors around an integer filling, $\nu = [i - \eta, i + \eta]$, where η is determined by the disorder, the Hall resistance is quantized to

$$R_{xy} = \frac{1}{i}\frac{h}{e^2} \text{ for } \nu = \frac{nh}{eB} = [i - \eta, i + \eta] \tag{2.12}$$

and the longitudinal resistance vanishes

$$R_{xx} = 0 \text{ for } \nu = \frac{nh}{eB} = [i - \eta, i + \eta] \tag{2.13}$$

We will refer to the plateau corresponding to the integer filling, i, as "the plateau of $\nu = i$". Along the whole plateau range, the number of chiral edge modes is i and the bulk is insulating.

2.3.4 Interactions

Finally, we discuss how electron-electron interactions modify and complete the above picture. As discussed in ref. [4], Coulomb interactions lead to a modification in the density distribution in an attempt to screen the disorder potential. Figure 2.8 demonstrates this effect. As seen in the figure, in regions where relatively small density variations can flatten the disorder potential, the highest occupied LL gets pinned to the Fermi energy and compressible regions are formed. These compressible regions are separated by incompressible regions where the density variations cannot screen the disorder potential, which leads to quantum dots formation. This modified picture of the nature of the localized states can lead to a significant differences from the simple single particle picture, for instance, to a number of localized states which is independent of the magnetic field (*i.e.* the LL degeneracy) [4].

Similarly, at the edges of the sample where the LLs bend upward due to the confining potential, such flattening also takes place. As described in ref. [5], this leads to a an alternating compressible and incompressible strips at the edge. In the compressible strips, the highest occupied LL is pinned to the Fermi energy, allowing the density to vary smoothly as the occupation of (extended) states is changed.

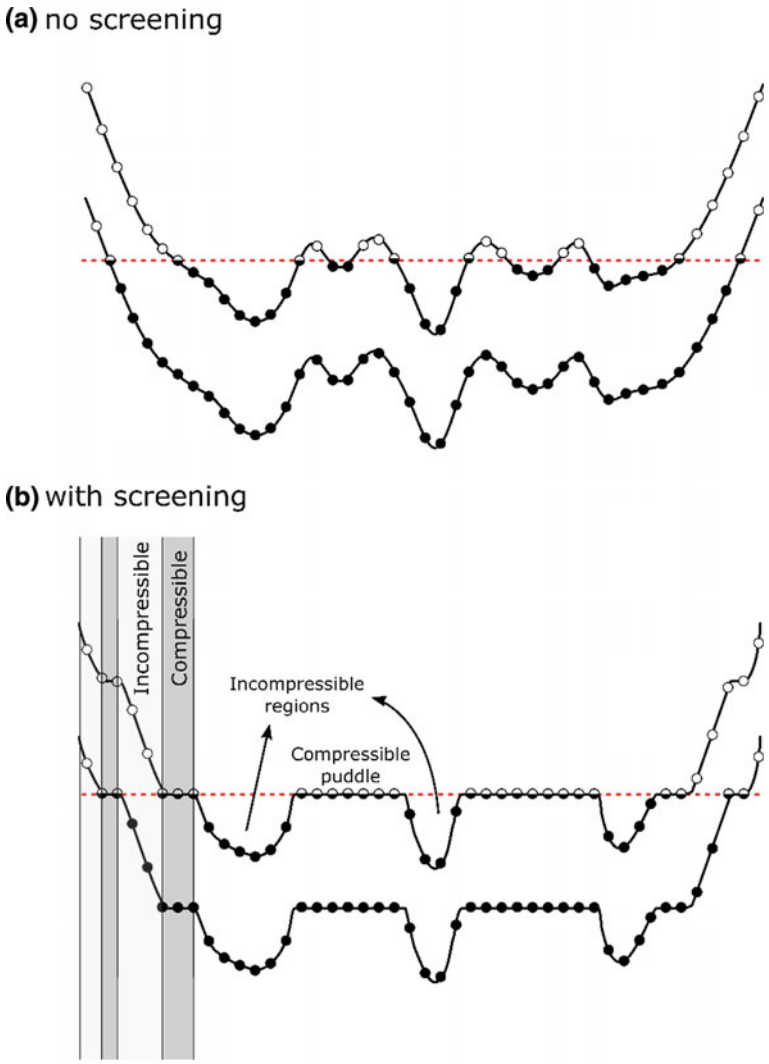

Fig. 2.8 LLs with disorder and coulomb interactions

2.4 Fractional Quantum Hall Effect

In 1982 Tsui, Stormer and Gossard [6] discovered a plateau at $\nu = 1/3$. With time, many more plateaus, accompanied by vanishing longitudinal resistance, were discovered at rational filling factors. This so called fractional quantum Hall effect (FQHE), cannot be explained by a simple non-interacting single particle picture and is rather a result of strong interactions. The $\nu = \frac{1}{3}$ plateau was theoretically

explained by Robert Laughlin in his famous ground state wave-function [7], for which he received the Nobel prize in 1998, together with Tsui and Stormer.

Several decades after the discovery of the FQHE, many open questions still remain and the FQHE is still a subject for ongoing research. For instance, the quasiparticle excitations in the FQHE are predicted to have exotic anyonic exchange statistics [8], which are yet to be observed. Moreover, as discussed above, the quasiparticles of the $\nu = 5/2$ FQHE state are expected to be MZMs with non-abelian exchange statistics [9]; a prediction which was strengthen by several recent experimental works [10–13]. Another important line of research is the probing and understanding of the particle-hole conjugate FQHE states, such as $\nu = 2/3$, which have neutral edge modes carrying quantized heat conductance and no charge [14–17]. Finally, as mentioned above and due to the predicted anionic nature of the FQHE excitations, it is theoretically predicted that when counter-propagating edge modes of a FQHE state, such as $\nu = 1/3$, that have opposite spins (*i.e.* fractional helical modes), are coupled to a conventional SC, a new topological SC would form hosting PFZMs [18].

In the work described below, we demonstrate for the first time the formation of fractional helical modes. Moreover, our novel platform serves as a new playground for research in the FQHE regime. For instance, we created an artificial $\nu = 2/3$ edge mode from counter-propagating $\nu = 1$ and $\nu = 1/3$ edge modes thus demonstrating some of the predicted universal behavior of such system [14, 15], and thus allowing access to a new regime that was previously inaccessible. Other possibilities, which will be discussed below, are designing novel edge mode interferometers with properties that may assist in probing fractional statistics, as well as engineering 'topological defects' that could exhibit anionic or even non-abelian statistics without superconductivity involved.

2.5 R_{xx} Versus B and V_G Measurement

In the following sections, we utilize samples that have a gate electrode, located on the surface of the heterostructure, called top gate (TG), as demonstrated in Fig. 2.9a, b. By varying the voltage on the TG the density in the 2DEG is varied. A 2D color plot of the longitudinal resistance, R_{xx}, as a function of magnetic field, B, and TG voltage, V_g, is shown in Fig. 2.9c. R_{xx} was measured by a 4-probe measurement, using a standard lock-in technique at a temperature of $\sim$20 mk. A series of finite R_{xx} lines, separated by $R_{xx} = 0$ lines can be seen. Following the above discussion, finite R_{xx} signifies that the Fermi energy is located in the extended states at the center of a LL, while $R_{xx} = 0$ signifies a QHE plateau (the Fermi energy is located in the localized states between two LL's centers), which corresponds to some integer filling factor, as indicated in the figure. The filling factors can be extracted either from the ratios of the magnetic fields in which $R_{xx} = 0$, or from a corresponding R_{xy} versus B and V_g-measurement.

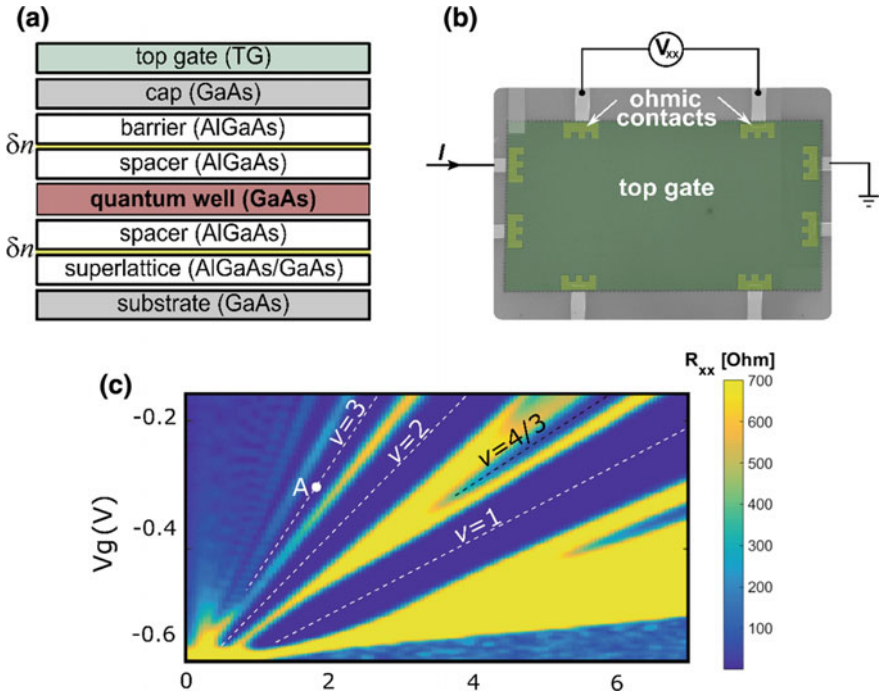

Fig. 2.9 Top gated devices and R_{xx} on the B-V_g plane. **a** A schematic diagram of the heterostructure with a top gate on the surface. **b** A top view SEM image of a Hall bar with a top gate covering it. The figure also illustrates the measurement scheme for **c**, where a color plot of R_{xx} as a function of magnetic field, B, and gate voltage, V_g, is shown

2.5.1 *The Slopes of the* $\mathbf{R_{xx}}$ *Lines*

To understand the slopes of the lines in Fig. 2.9c, let's follow the $\nu = i$ lines (i, integer), shown in white dashed lines. When the magnetic field is changed by ΔB, the degeneracy of each LL is changed by $\frac{\Delta B}{\phi_0}$ (per unit area). In order to stay on a $\nu = i$ line, the density must increase by $\Delta n = i\frac{\Delta B}{\phi_0}$; thus, the slope of the $\nu = i$ line is proportional to $\frac{\Delta V_g}{\Delta B} = \frac{e\Delta n}{C_g \Delta B} = \frac{i}{\phi_0}$, with C_g the gate-2DEG capacitance. The slope of the $\nu = 3$ line, for example, is three times larger than the slope of the $\nu = 1$ line (assuming constant gate-2DEG capacitance).

2.5.2 *The Width of the* $\mathbf{R_{xx}}$ *Lines*

The widths of the finite R_{xx} lines is determined by the width of the QHE plteaus. The wider the plateaus, the narrower the finite R_{xx} lines. As discussed above this is

related to the number of localized and extended states in the bulk of each LL. To transition from the $v = i-1$ plateau to the $v = i$ plateau, all of the extended states of the i_{th} LL must be filled. Since the vertical axis is proportional to the density, the vertical width of the finite R_{xx} line between the $v = i-1$ plateau and the $v = i$, corresponds to the density change which is needed to fill these extended states.

2.5.3 *FQHE States in the* $\mathbf{R_{xx}}$ *Color Plot*

What about FQHE states? As can be seen in Fig. 2.9c, the finite R_{xx} lines of the low order LLs split, and new $R_{xx} = 0$ regions appear due to FQHE states. The black dashed line in the figure indicates the v = 4/3 FQHE state. As the magnetic field and the density (gate voltage) increase, the fractional states become more pronounced with wider $R_{xx} = 0$ regions. Note that the sample shown in Fig. 2.9 has a relatively low mobility and hence, not many FQHE states are seen. As will be shown below, higher mobility samples show a richer pattern of fractional states.

2.6 Edge Mode Devices

Edge modes are not limited to emerge only at the physical edge of the 2DEG. By shaping various kinds of TGs and gating specifically defined regions of a 2DEG, edge modes can be formed at the edges of a TG or in the interface between two TGs. For instance, if two TGs are made in the geometry shown in Fig. 2.10, with the region under the left TG tuned to $v = 3$ while the region under the right TG tuned to $v = 1$, two edge modes flow on the interface, as illustrated in the figure. However, as we now discuss, in order to utilize QHE edge modes to form helical modes, a simple 2DEG is not enough. A new degree of freedom must be introduced.

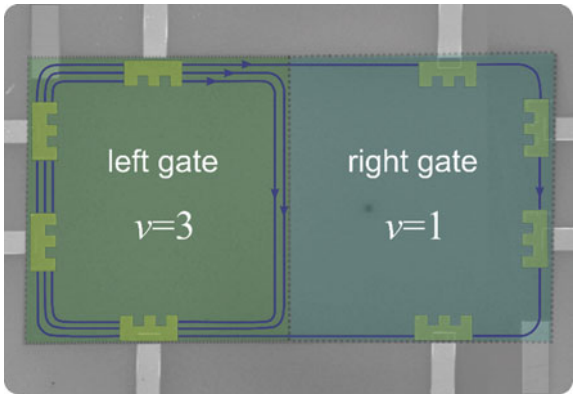

Fig. 2.10 Edge states in the interface between to top gates. The left top gate is set so that the filling factor underneath is v = 3 while the right top gate is set so that the filling factor underneath is v = 1. Thus two edge modes form in the interface

References

1. Umansky, V., Heiblum, M.: MBE growth of high-mobility 2DEG. In: Molecular Beam Epitaxy, 121–137. Elsevier (2013) https://doi.org/10.1016/b978-0-12-387839-7.00006-3
2. Hall, E.H.: On a new action of the magnet on electric currents. Source Am. J. Math. **2**, 287–292 (1879)
3. Klitzing, K. V., Dorda, G., Pepper, M.: New method for high-accuracy determination of the fine-structure constant based on quantized Hall resistance. Phys. Rev. Lett. **45,** 494–497 (1980)
4. Ilani, S., et al.: The microscopic nature of localization in the quantum Hall effect. Nature **427**, 328–332 (2004)
5. Chklovskii, D.B., Shklovskii, B.I., Glazman, L.I.: Electrostatics of edge channels. Phys. Rev. B **46**, 4026–4034 (1992)
6. Tsui, D.C., Stormer, H.L., Gossard, A.C.: Two-dimensional magnetotransport in the extreme quantum limit. Phys. Rev. Lett. **48**, 1559–1562 (1982)
7. Laughlin, R.B.: Anomalous quantum hall effect: an incompressible quantum fluid with fractionally charged excitations. Phys. Rev. Lett. **50**, 1395–1398 (1983)
8. Wilczek, F.: Magnetic flux, angular momentum, and statistics. Phys. Rev. Lett. **48**, 1144–1146 (1982)
9. Moore, G., Read, N.: Nonabelions in the fractional quantum Hall effect. Nucl. Phys. B **360**, 362–396 (1991)
10. Dolev, M., Heiblum, M., Umansky, V., Stern, A., Mahalu, D.: Observation of a quarter of an electron charge at the $\nu = 5/2$ quantum Hall state. Nature **452**, 829–834 (2008)
11. Bid, A., et al.: Observation of neutral modes in the fractional quantum Hall effect regime. In: AIP Conference Proceedings **1399,** 633–634 (2011)
12. Willett, R. L., Pfeiffer, L. N., West, K. W.: Measurement of filling factor 5/2 quasiparticle interference with observation of charge e/4 and e/2 period oscillations. Proc. Natl. Acad. Sci. U. S. A. **106,** 8853–8 (2009)
13. Banerjee, M., et al.: Observation of half-integer thermal Hall conductance. arXiv:1710.00492 (2017)
14. Kane, C.L., Fisher, M.P.A., Polchinski, J.: Randomness at the edge: theory of quantum Hall transport at filling $\nu = 2/3$. Phys. Rev. Lett. **72**, 4129–4132 (1994)
15. Protopopov, I.V., Gefen, Y., Mirlin, A.D.: Transport in a disordered $\nu = 2/3$ fractional quantum Hall junction. Ann. Phys. (N. Y) **385**, 287–327 (2017)
16. Bid, A., et al.: Observation of neutral modes in the fractional quantum Hall regime. Nature **466** (2010)
17. Inoue, H., et al.: Proliferation of neutral modes in fractional quantum Hall states. Nat. Commun. **5**, 4067 (2014)
18. Clarke, D.J., Alicea, J., Shtengel, K.: Exotic non-abelian anyons from conventional fractional quantum Hall states. Nat. Commun. **4**, 1348 (2013)

Chapter 3
Two Subbands Quantum Hall System as a Platform for Edge Mode Manipulations

It is natural to ask whether it is possible to use the edge modes of the IQHE and FQHE to create 1D integer helical and factional helical modes. The QHE edge modes are extremely robust and moreover, as discussed above, they can be manipulated to form complicated structures using standard lithographic techniques. However, a difficulty to create counter-propagating edge modes is apparent, since the QHE edge modes propagate in the same chiral direction. One can try to overcome this by separating two QHE regions of, say $\nu = 1$, with a thin regions of, say $\nu = 0$, as shown in Fig. 3.1 (this can be done, for example, by gating the center region [1]). However, the two counter-propagating edges that result from this have the same spin and therefore do not form helical modes. Note also that it would be impossible to bring the two edges very close to each other due to both fabrication limitation as well as since the two edge states will then simply hybridize.

To overcome this, we employ a double-quantum-well system that hosts two electronic sub-bands, as we now describe.

3.1 Double Quantum Well

Figure 3.2 shows a schematic diagram of a double quantum well heterostructure where two GaAs layers are separated by a thin AlGaAs layer that forms a potential barrier in the center of the well. The figure corresponds to a heterostructure we denote as *DQWa* for which we present results. Here the GaAs well is 40 nm wide and the AlAs barrier in its center is 3 nm wide. The double well potential, which is formed due to this structure is shown in the right panel of Fig. 3.2. The figure shows results of a NextNano3 simulation, which takes into account the MBE growth parameters as well as the voltage of a top gate. The figure also shows the simulation results for the total densities in the upper and lower regions of the double well, as well as the density distribution in the 1st and 2nd electronic subbands of the well. We denote these subbands by SB_1 and SB_2. Since there is a finite charge

Y. Cohen, *A New Platform for Edge Mode Manipulations in the Quantum Hall Effect*, Springer Theses, https://doi.org/10.1007/978-3-030-05943-9_3

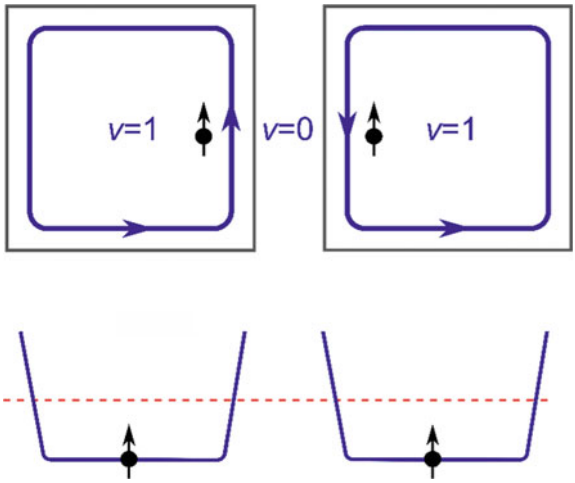

Fig. 3.1 Counter-propagating edge modes in a single 2DEG QHE must be of the same spin

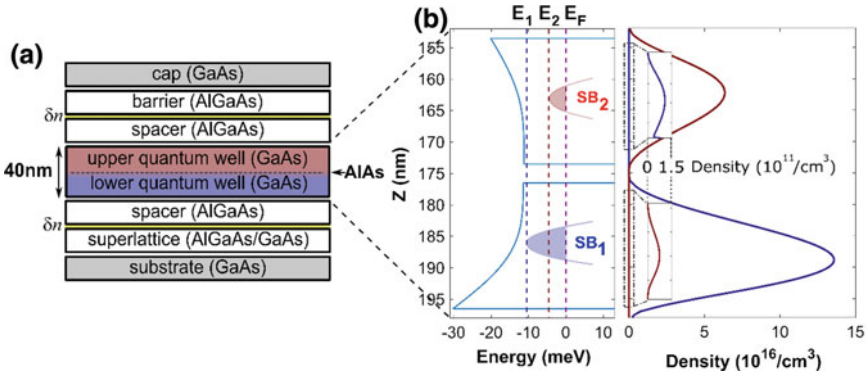

Fig. 3.2 Double quantum well. **a** A schematic diagram of the DQWa heterostructure. A thin, 3 nm AlAs layer is grown in the center of the 40 nm wide GaAs quantum well to form a double quantum well potential. **b** The left panel shows a nextnano3 simulation of the bottom of the conduction band which forms the double well potential in the GaAs region of the heterostructure. The energies of the subbands as well as the Fermi energy are indicate by the dashed lines. The right panel shows the density distribution of each subband illustrating that in this case most of the density of SB_1 is located in the lower side of the well while most of the density of SB_2 is located in the upper side of the well

density both subbanda, each subband hosts its own 2DEG which in high magnetic field develops its own LLs. There are therefore two filling factors: v_1 for SB_1 and v_2 for SB_2. We define a generalized filling factor by

$$v = (v_1, v_2)$$

3.2 Forming Helical Modes—The Concept

Figure 3.3 illustrates schematically how the addition of the subband degree of freedom allows the formation of helical edge modes. The sub-bands, are depicted as two 2-dimensional sheets (blue for SB_1 and red for SB_2) and each SB has its own edge modes according to its filling factor. Figures 3.3a, b describe the scenarios of $v = (2, 0)$ and $v = (1, 1)$, respectively. If these two configurations can be placed one next to the other in the same sample, as shown in Fig. 3.3c, counter-propagating chiral edge modes with opposite spins would propagate along the interface. The opposite spins are due to the fact that the two edge modes in the interface are the edge modes of LL2 in SB_1 (spin down) and the edge mode of LL1 in SB_2 (spin up). Note that the edge mode of LL1 in SB_1 circulates around the edge of the whole sample since this LL is filled in the whole sample.

The pair of filling factors (2, 0) and (1, 1) is not the only one which will result in helical modes. For instance, the filling factors (4, 0) and (3, 1) will give a similar result. On the other hand, the interface between (3, 0) and (2, 1) will result in counter-propagating edge sates with the same spin. In general, $(2n, 2m)$ to $(2n + 1,$

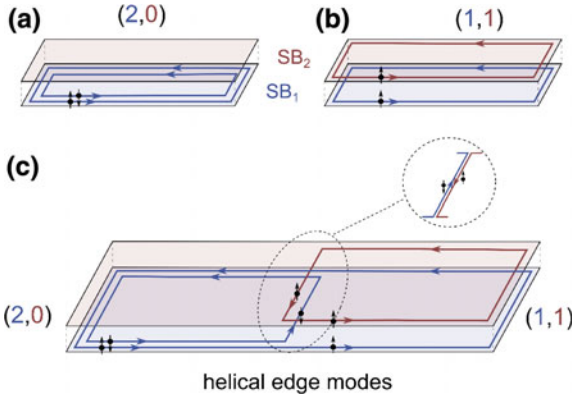

Fig. 3.3 Schematic illustration of the concept of creating helical edge modes in a double-layer quantum Hall effect system. The two subbands, SB_1 and SB_2, are shown in blue and red, respectively. Each subband has its own filling factor, v_1 and v_2, respectively with the generalized filling denoted by $v = (v_1, v_2)$, **a** Scenario of $v = (2,0)$, with two edge modes propagating at the edge of SB1. **b** Scenario of $v = (1, 1)$,, with one edge modes propagating at the edge of SB1 and one at the edge of SB2. **c** The left half-plane is in $v = (2, 0)$ and the right half-plane is in $v = (1, 1)$. This creates counter-propagating edge modes with opposite spins at the interface between the two half-planes (see inset)

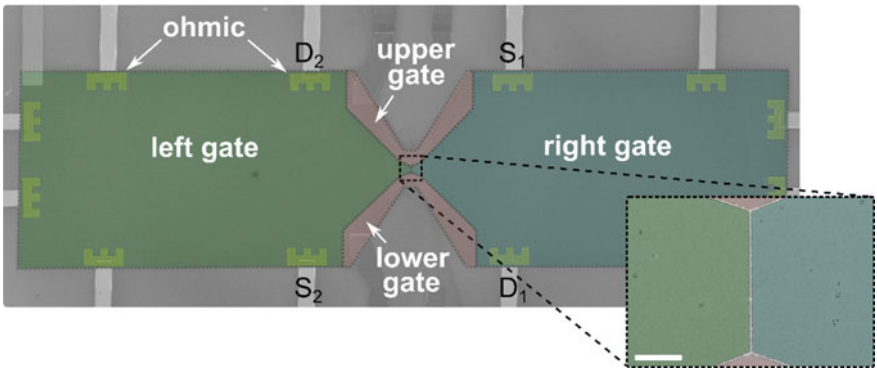

Fig. 3.4 Device A. The figure shows a false colors SEM image of the device. Mesa size is 800 μm long and 200 μm wide with a narrower region which is 7 μm wide in the center, where the left and right top gates interface. The inset shows a zoom on the interface between the left and right top gates where the helical edge modes are designed to emerge (scale-bar 2 μm). Note, the two additional upper and lower gates allow changing the filling factors configurations and thus changing the propagation length of the counter-propagating modes

$2m + 1$) transitions will lead to modes with opposite spins, while $(2n - 1, 2m)$ to $(2n, 2m + 1)$ transitions will lead to modes with the same spins.

A top-view SEM image of the device we used to implement this idea is shown in Fig. 3.4. We will denote this device as *device A*. Two top-gates divide the surface to two adjacent half-planes. The inset shows a zoom on the interface between the left and right top gates where the helical edge modes are designed to emerge (scale-bar 2 μm). There are in fact two additional gates, which allow changing the configurations and thus control the propagation length of the counter-propagating modes. However, it is not trivial that we can change the filling factor from (n, m) to $(n + 1, m - 1)$ by using TGs voltages alone.

The fan diagram for the two subbands quantum Hall system is shown in Fig. 3.5. The LLs of SB_2 are shifted from the LLs of SB_1 by the SBs energy separation, ΔE_{SB}. Since the slope of lower LLs (e.g. LL1, LL2) is smaller than the slop of higher LLs (e.g. LL3, LL4), as the magnetic field is increased, the lower LLs of SB_2 cross the higher LLs of SB_1. At each point on the *E-B* plane, the filling factor of SB_1 (SB_2) can be found by counting the number of blue (red) lines below it. For example, below point A there are two blue lines and no red lines so that the generalized filling factor is $\nu = (2, 0)$. Below point B, on the other hand, there is one blue lines and one red line, so that $\nu = (1, 1)$.

Figure 3.5 seems to present a serious problem. The two filling factors, (2, 0) and (1, 1), do not seem to coexist in the same magnetic field. While electrostatic gating of different regions of the Hall bar is straight forward, it is not possible to change the magnetic field locally. Another related problem that comes to mind, is that in the transition from (2, 0) to (1, 1), the density in SB_1 must decrease to change the filling factor from 2 to 1, while the density in SB_2 must increase to change the filling from 0 to 1. How can this be done using only the TG voltage?

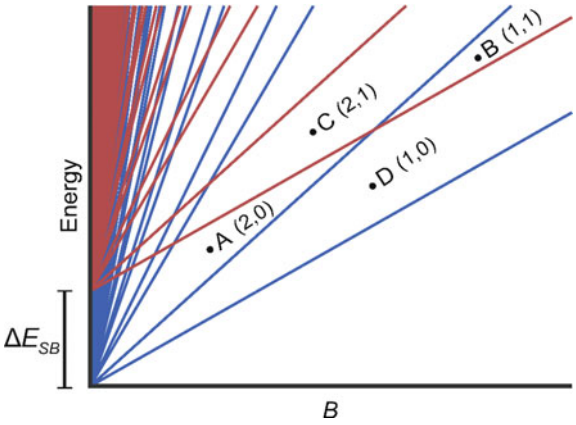

Fig. 3.5 Two subbands fan diagram. The Landau levels of the first subband (blue) and the second subband (red) are separated by an energy gap ΔE_{SB}, which leads to level crossings

Fortunately, there is more to the TG than meets the eye. Since the gate voltage actually affects the relative energies of the two SBs (and thus affects the fan diagram itself), it turns out that under certain conditions, the transition between the desired filling factors can be achieved by tuning only the TG voltage. The reason for this will be discussed in detail in Sect. 4, but first, let's see the end result.

3.3 Forming Helical Modes—The Execution

Figure 3.6a shows the R_{xx} color plot on the B-V_g plane for *device A*. This measurement and all subsequent measurements were taken using a standard lock-in technique at a temperature of $\sim$20 mK. While the transition (2, 0)-(1, 1) cannot be driven only by gate voltage, other transitions which give helical modes such as (4, 0)-(3, 1) can! This can be seen clearly from Fig. 3.6b, which zooms in on the (4, 0)-(3, 1) transition. At B = 2.275T, if the left and right gate voltages of the device (Figs. 3.4 and 3.6c) are tuned to point A (yellow) and B (green), respectively, we expect helical modes to emerge in the interface.

To observe this, the following experiment is performed. The left gate voltage, V_{LG}, is tuned to point A (yellow) of Fig. 3.6b, while the right gate voltage, V_{LG}, is scanned along the black arrow shown in the figure. Thus, the filling factor of the left half-plane is (4, 0), while the filling factor of the right half-plane changes from (3, 0) $\rightarrow$ (4, 0) $\rightarrow$ (3, 1) (Fig. 3.6c). A current of 1nA is injected at S_1 and its reflected part, $I_{S1\rightarrow D1}$, is plotted in Fig. 3.6d (upper panel). With the left half-plane at (4, 0), and the right half-plane tuned to (3, 0) or (4, 0), all the injected edge modes continue along the upper edge and arrive at D_2 while $I_{S1\rightarrow D1} = 0$. When the right half-plane is tuned to (3, 1), three edge modes arrive at D_2 while one edge mode (LL1 in SB_2, red Fig. 3.6c) is then fully reflected to D_1, with $I_{S1\rightarrow D1}$ = 0.25 nA.

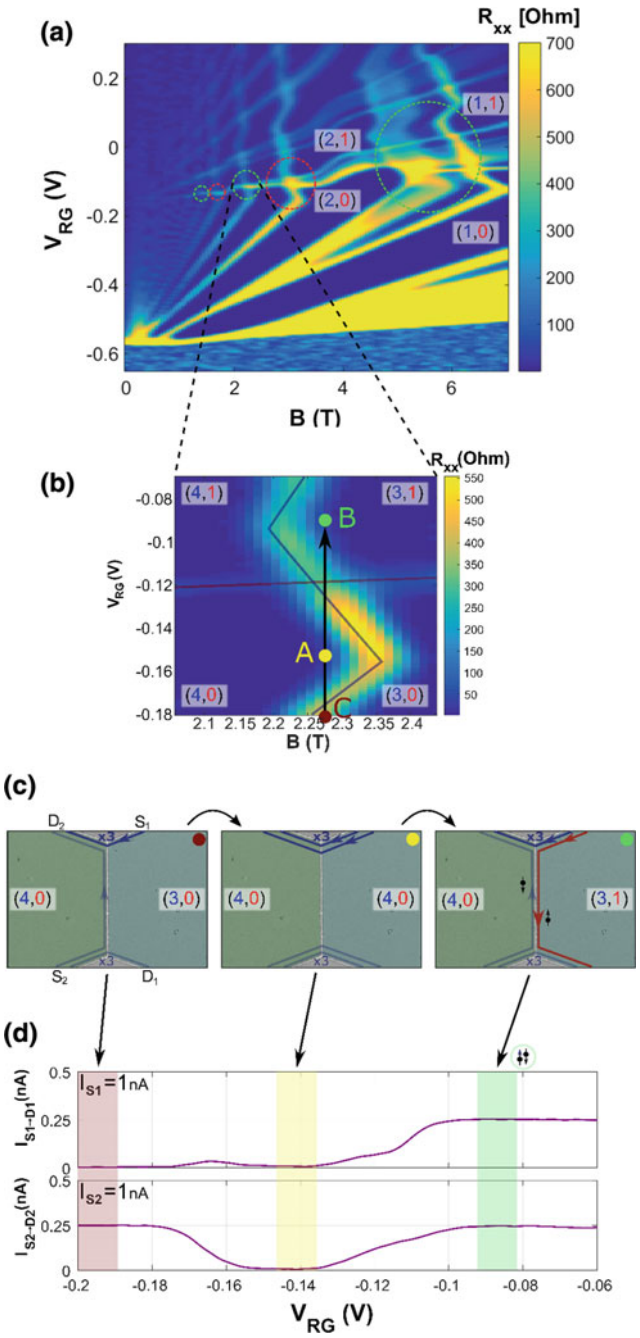

Fig. 3.6 Forming helical modes in a two subbands quantum Hall system

Similarly, injecting current at S_2 and measuring $I_{S2\rightarrow D2}$, leads to a complimentary result (Fig. 3.6d, lower panel). Therefore, in the helical modes configuration, we observe ballistic transport along the gates' interface both in the downward and upward direction (Fig. 3.6d, green shaded region), agreeing with counter-propagation of helical modes without inter-mode scattering.

As mentioned above, other transitions can be used to form helical edge modes as well as same-spin counter-propagating edge modes. In Fig. 3.7 $I_{S1\rightarrow D1}$ is plotted for the four possible transitions in *Device A*. For each transition three traces are shown corresponding to three different counter-propagation lengths, L_{CP} = 7 μm, 150, and 300 μm. A clear difference is observed between same-spin transitions (*odd*, 0) → (*even*, 1) and opposite-spin transitions (*even*, 0) → (*odd*, 1). In the former case, as L_{CP} increases beyond 7 μm a reduction in $I_{S1\rightarrow D1}$ is observed (Fig. 3.7a, c). This reduction is fully compensated by an increase in $I_{S1\rightarrow D2}$, as shown in Fig. 3.8, proving that inter-mode equilibration takes place (due to tunneling). In contrast, when helical modes are formed, no reduction in $I_{S1\rightarrow D1}$ is observed, even for L_{CP} = 300 μm—demonstrating spin protection against inter-mode tunneling. Figure 3.9 shows that there is also in increase in $I_{S1\rightarrow D2}$ to fully complete the picture. Finally, Fig. 3.10 shows the extracted transmission of the counter propagating channels as a function of the propagation length for the four different filling factors configurations.

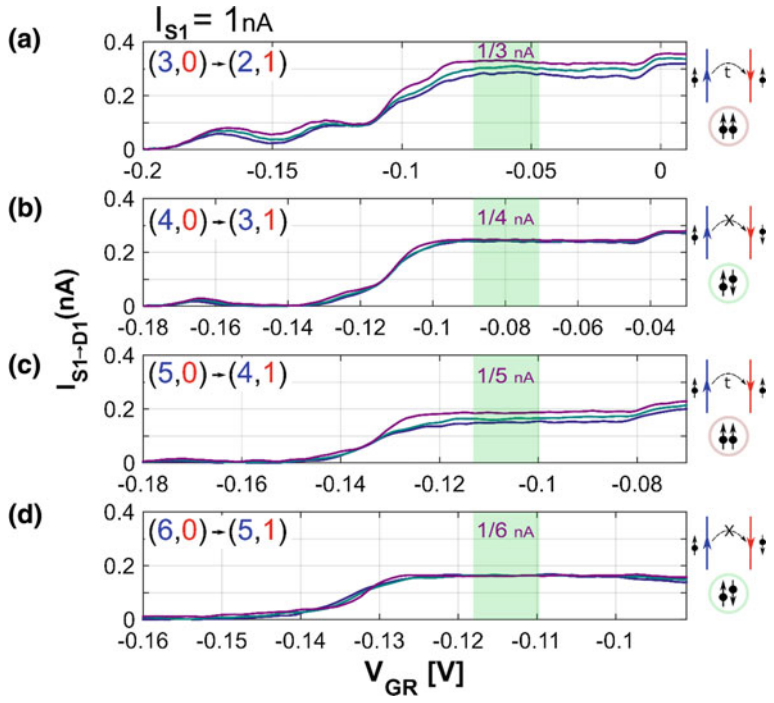

Fig. 3.7 Spin protection and inter-mode tunneling in counter propagating modes. In the opposite spins configurations (helical modes), strong protection against inter-mode tunneling is observed, compared to the same spins configurations

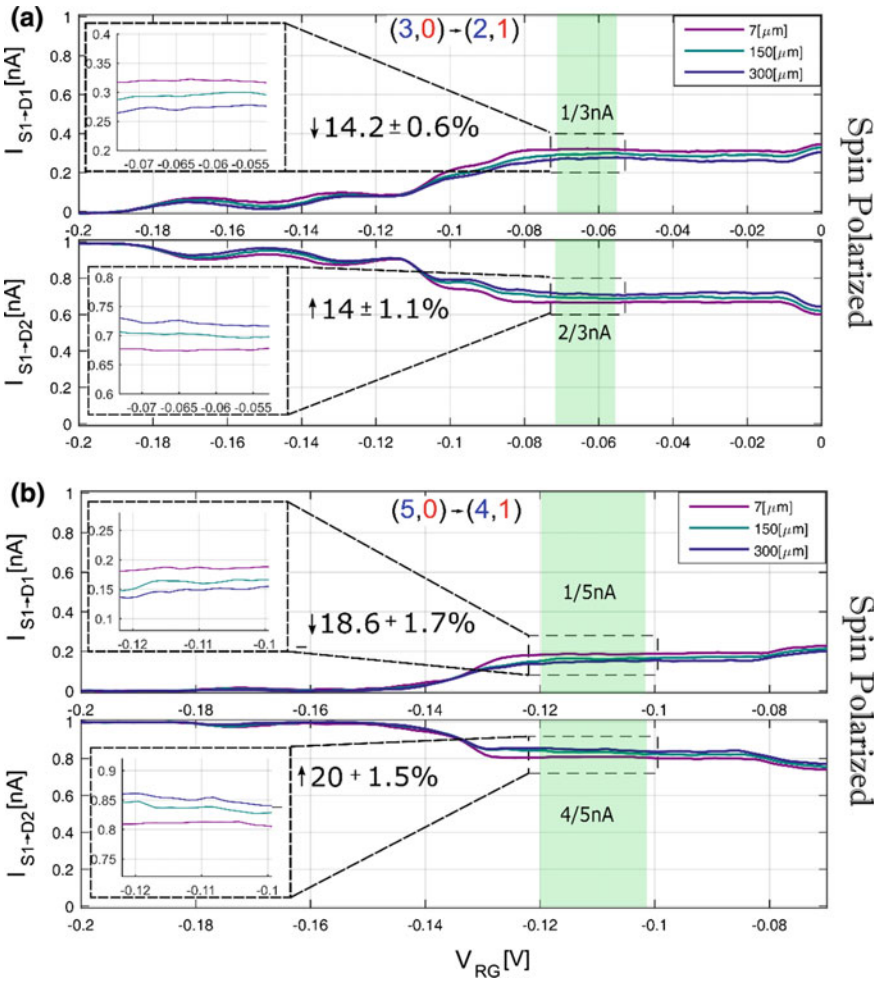

Fig. 3.8 Full details on inter-mode tunneling in the same spin counter-propagating modes configurations. The reduction in $I_{S1\to D1}$ is shown to be compensated by an increase in $I_{S1\to D2}$, demonstrating that this reduction is indeed due to inter-mode tunneling

3.4 Detailed Discussion of the Filling Factors Transition

The possibility to induce the desired filling factor transitions ((n, m) to (n + 1, m − 1)) by top gate manipulation alone is a result of an interplay between several effects that we now discuss in detail.

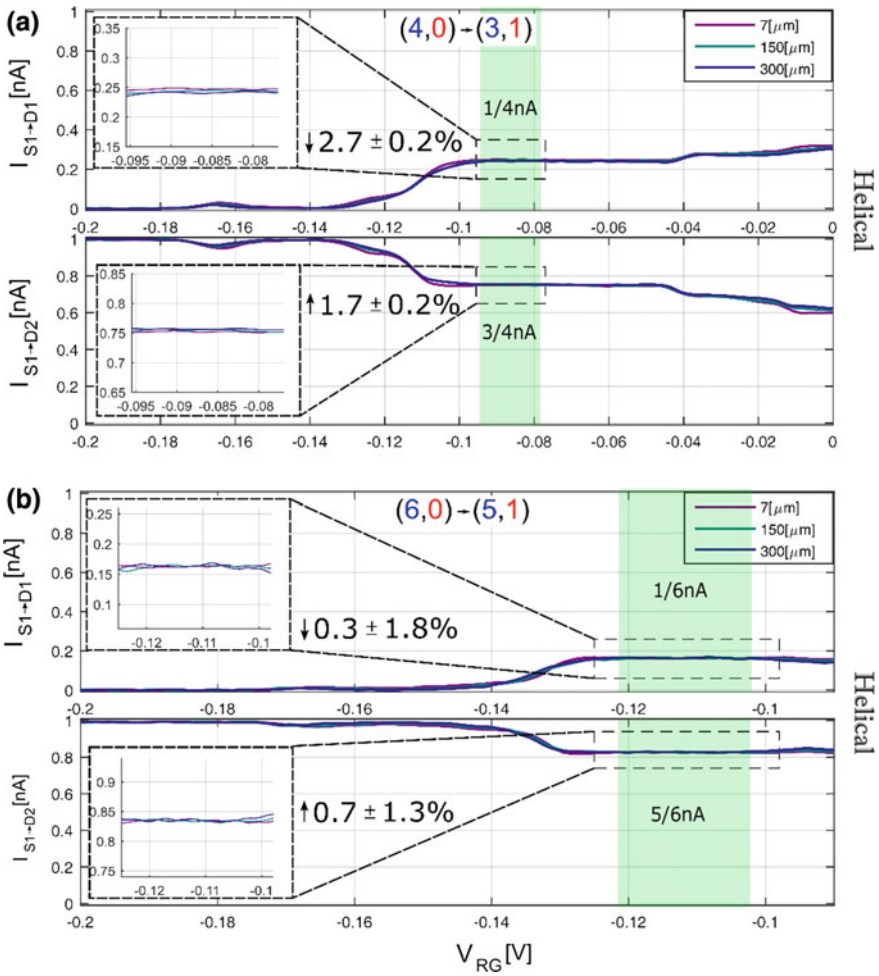

Fig. 3.9 Full details on spin protection in the helical modes configurations

3.4.1 Localized States and Partial Filling on QHE Plateaus

As mentioned in the discussion of the QHE, the localized bulk states resulting from the disorder potential are crucial for observing QHE plateaus. The filling factors of points such as A and B in Fig. 3.6b are evidently not really integer fillings, but rather fractional fillings in which the system is in a QHE plateau. Point A, for example, could be in $\nu = (3.76, 0.03)$ which is on the $\nu = (4, 0)$ QHE plateau, while point B in $\nu = (3.25, 0.94)$ which is on the $\nu = (3, 1)$ QHE plateau. While this does not have a significant effect on the edge states picture, and thus on the helical modes formation, it is central for understanding the LLs crossing regions of Fig. 3.6a, b.

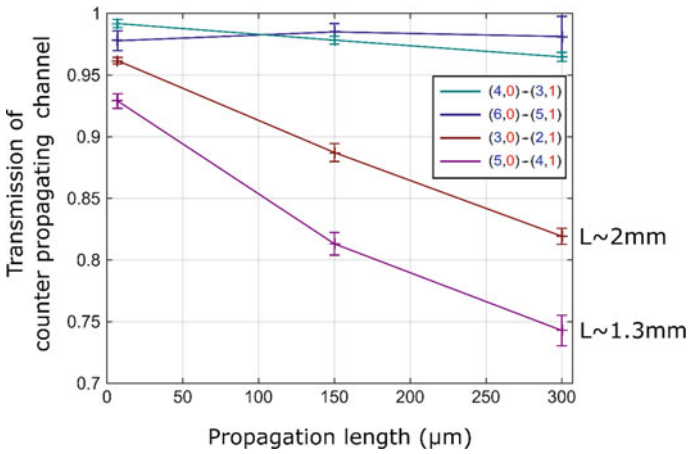

Fig. 3.10 Transmission of the counter propagating channels as a function of propagation length for various filling factors configurations

The localized states can already give a partial answer to an important issue. Since the gate voltage changes the total density, it changes the total filling factor $\nu_T = \nu_1+\nu_2$. It is therefore impossible to transition from $\nu = (4, 0)$ to $\nu = (3, 1)$, both of which have the same total filling factor, by changing the gate voltage alone at a fixed magnetic field. On the other hand, the transition from $\nu = (3.74, 0.03)$ to $\nu = (3.28, 0.89)$ may be possible since the total filling factors are $\nu_T = 3.77$ and $\nu_T = 4.17$. Our next task now, is to explain how changing the gate voltage increases the filling factor in one SB and decreases it in the other.

3.4.2 *Gate Induced LLs Crossing and Inter-Subband Charge Transfer*

Since the TG is located on the surface of the heterostructure, closer to the upper quantum well (see Fig. 3.2) it affects the shape of the DQW in an asymmetric way. As shown in Fig. 3.11a, when the gate voltage increases, it pulls down the upper side of the well relative to the lower side, making the well more symmetric and therefore reducing the subbands energy separation, ΔE_{SB}. In turn, all the LLS of SB_2 are shifted downward compared to those of SB_1, which can lead to a gate induced LLs crossings, as shown in Fig. 3.11b.

Due to the LLs crossing, when states of, say, LL1 of SB_2 become lower in energy than states of, say, LL4 of SB_1, electrons that filled the former are poured into the latter (Fig. 3.11b) [2, 3]. This inter-subband charge transfer decreases the filling factor of SB_1, while it increases the filling factor of SB_2, exactly as needed! This explains why in the LLs crossing regions of Fig. 3.6a, b, the finite R_{xx} lines of

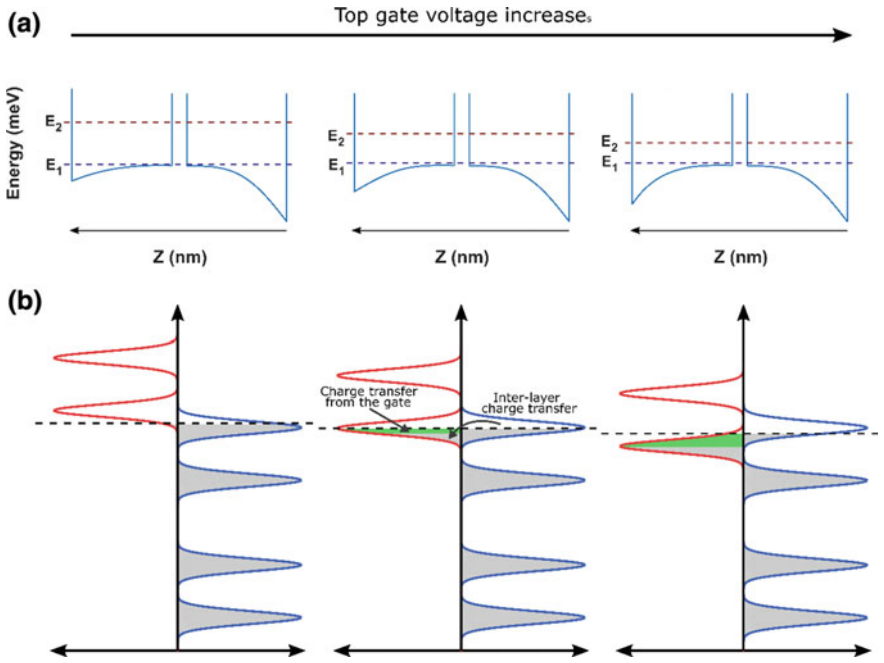

Fig. 3.11 Gate induced Landau levels crossing and inter-layer charge transfer

SB_1 bend towards lower magnetic fields when the gate voltage is increased. The higher the gate voltage, the lower the filling factor of SB_1, which means that to keep the same filling the magnetic field must be decreased.

Two important comments must be made regarding this effect. First, as noted above, increasing the gate voltage evidently also increases the total density. As long as SB_2 has a large enough density of states around the Fermi energy, this extra density goes almost entirely to SB_2 (green region in Fig. 3.11b), as it screens the gate to SB_1. Only when the LL crossing is almost over, and the very low density of states tale of SB_2's LL is at the Fermi energy, does increasing the gate voltage fills SB_1 again (Fig. 3.11b right image). Second, the amount of inter-subband charge transfer for a given change in gate voltage, ΔV_g, depends on the density of states around the Fermi energy, which in turn depends on the LLs broadening. If, for example, the LLs broadening is very large, the density of states is lower and the charge transfer is slower and spreads over a wider range of gate voltage. This makes the 'bending angle' of the finite R_{xx} lines at the crossing more moderate. The possibility of making the desired filling factor transition by changing the gate voltage only depends on the interplay between the angle of the R_{xx} lines and their width.

3.4.3 Following the Gate Induced LLs Crossing

Figure 3.12 shows a simulation of an R_{xx} color plot around a crossing point. The simulation assumes a very large amount of localized states ($\sim$90% of LLs degeneracy) as well as very small LLs broadening ($\sim$5% of $\hbar\omega_c$). Let's follow closely the points on the black arrow in the figure:

- Point A: ν = (3.55, 0.00), ν_T = 3.55. This is just on the edge of the ν = (4, 0) plateau since all of the extended states of LL4 of SB_1 are filled while no localized states are filled.
- Point B: ν = (3.67, 0.02), ν_T = 3.69. LLs crossing started. Note that the density of states of SB_2 near the Fermi energy is still very low and thus SB_1 is still being filled by the gate.
- Point C: ν = (3.55, 0.24), ν_T = 3.79. When the gate voltage is increased to reach point C, electrons are transferred from SB_1 to SB_2. In addition, some extra charge is added to SB_2 from the gate. Therefore, while the total filling factor increased from point B, the filling factor of SB_1 decreased. We are now again on the edge of the (4, 0) plateau since the Fermi energy is in the extended states of LL4 of SB_1.
- Point D: ν = (3.45, 0.39), ν_T = 3.84. All of the extended states of LL4 of SB_1 are emptied due to inter-layer charge transfer and we are now entering the ν = (3, 0) QHE plateau.
- Point E: ν = (3.42, 0.45), ν_T = 3.87. This is the edge of the ν = (3, 0) plateau since all of the localized states of LL1 of SB_2 are now filled and the next states to fill are extended states.
- Point F: ν = (3.36, 0.55), ν_T = 3.91. All of the extended states of LL1 of SB_2 are now filled and we enter the plateau of ν = (3, 1).
- Point G: ν = (3.22, 0.77), ν_T = 3.99. On the ν = (3, 1) plateau. LLs crossing still continues so that LL1 of SB_2 is being filled while LL4 of SB_1 is being emptied.
- Point H: ν = (3.15, 0.99), ν_T = 4.14. On the ν = (3, 1) plateau. LL1 of SB_2 is now almost full and its density of states near the Fermi energy is very small. Therefore, from now on the gate voltage increase will fill LL4 of SB_1.

Of course, this journey would have been different if we went along the white arrow in the figure. For instance, point A′ is at the same gate voltage as point A, but at lower magnetic field. Therefore, the energy difference between the LLs in point A′ is larger than that of point A. In addition, the degeneracy of the LLs is therefore smaller so instead of starting at A: ν = (3.55, 0.00), we start at A′: ν = (3.78, 0.00). Then, as can be seen in the figure, we hit the extended states of LL1 of SB_2 before we hit the extended states of LL4 of SB_1 (point C′) and therefore the order of the lines switch. Finally, the plateau between the lines is now (4, 1) (point D′) and not (3, 0) as before.

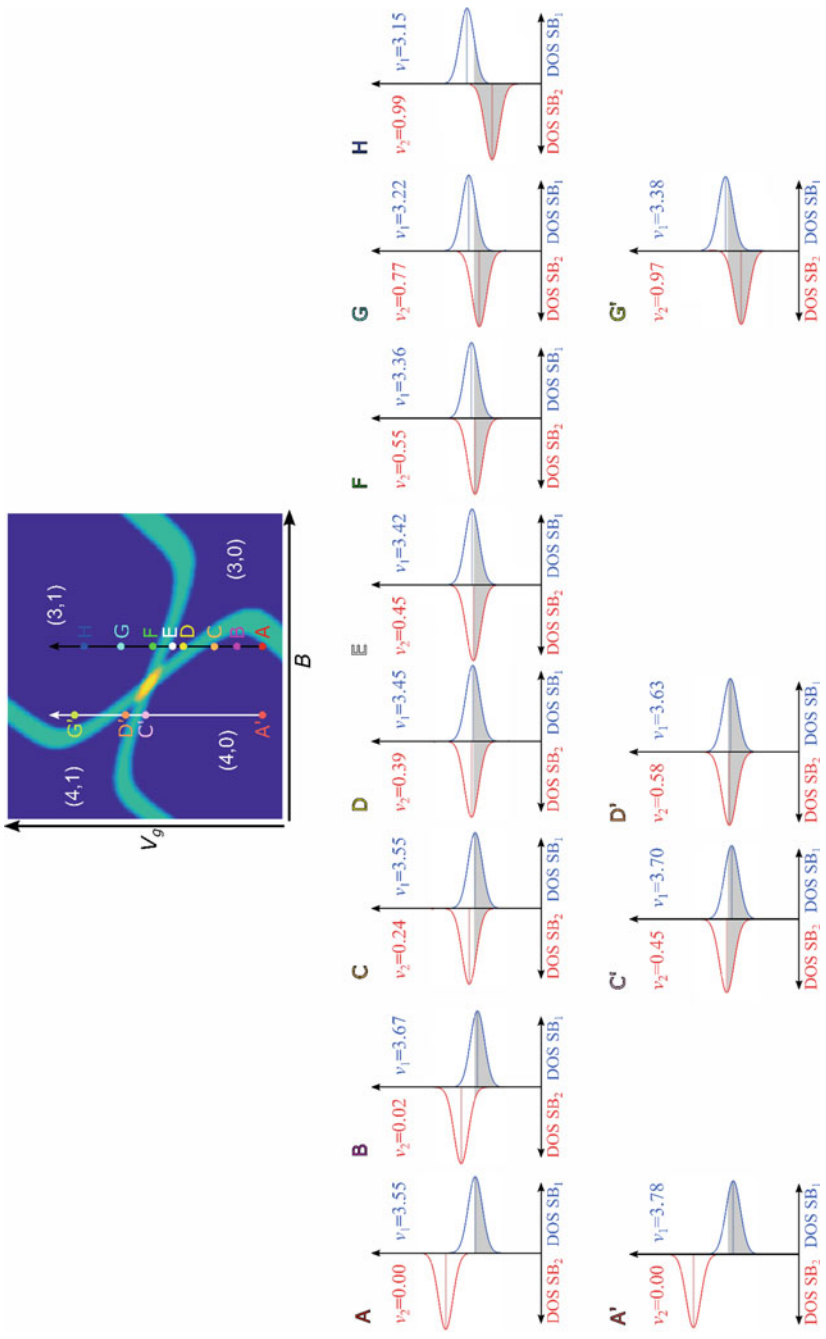

Fig. 3.12 Following the LLs crossing

3.4.4 The Charging Energy Effect

There is yet another important effect that was omitted from the picture described above, which must be mentioned. Due to the spatial separation between the densities in the two SBs, the inter-subband charge transfer introduces an additional charging energy, which actually resists the charge transfer [2]. We can view the two SBs as an effective parallel plate capacitor. When the gate induces LLs crossing and charge is transferred from, say, LL4 of SB_1 to LL1 of SB_2, this 'capacitor' is charged. The charging energy pushes LL1 of SB_2 up and LL4 of SB_1 down and the result is a smaller net charge transfer for a given change in gate voltage, ΔV_g. Thus, the smaller the mutual capacitance between the two subbands, the less bending of the finite R_{xx} lines. To diminish this effect, the full width of the DQW must be minimized, while the inter-subband tunneling is controlled by the AlAs barrier.

3.4.5 Combining It All

Figure 3.12 assumes a very small extended to localized states ratio, namely a very small LLs broadening[1] and a very large mutual capacitance between the subbands (small charging energy). In Fig. 3.13 we illustrate how the picture would look like with various amounts of broadening, localized states and inter-subband charging energy.

3.5 Manipulating the Laterar Distance Between Counter-Propagating Edge Modes

Let's examine what happens across the interface between two TGs, such as the ones shown in Fig. 3.14. The 2DEG is typically $\sim$100 nm below the TGs and thus the potential at the 2DEG level changes gradually along $\sim$100 nm. If the left and right gate voltages and the magnetic field are tuned to points A (or A′ or A″) and B (or B′ or B″) in the figure, respectively, the LLs cross each other somewhere at the interface as well as cross the Fermi energy, thus forming two counter-propagating edge modes (Fig. 3.14c). However, only for the A′-B′ transition, the two LLs cross the Fermi energy exactly when they cross each other leading to the two counter-propagating edge modes being in the same position along the x-axis (Fig. 3.14c, middle image). On the other hand, for the A-B transition, the LL of SB_1

[1]Note that usually, these do not go together as adding disorder typically lowers the extended to localized states ratio but broadens the levels. The kind of disorder which achieves this would an many relatively small hills and valleys to the potential landscape so that there are more localized states but not too much broadening.

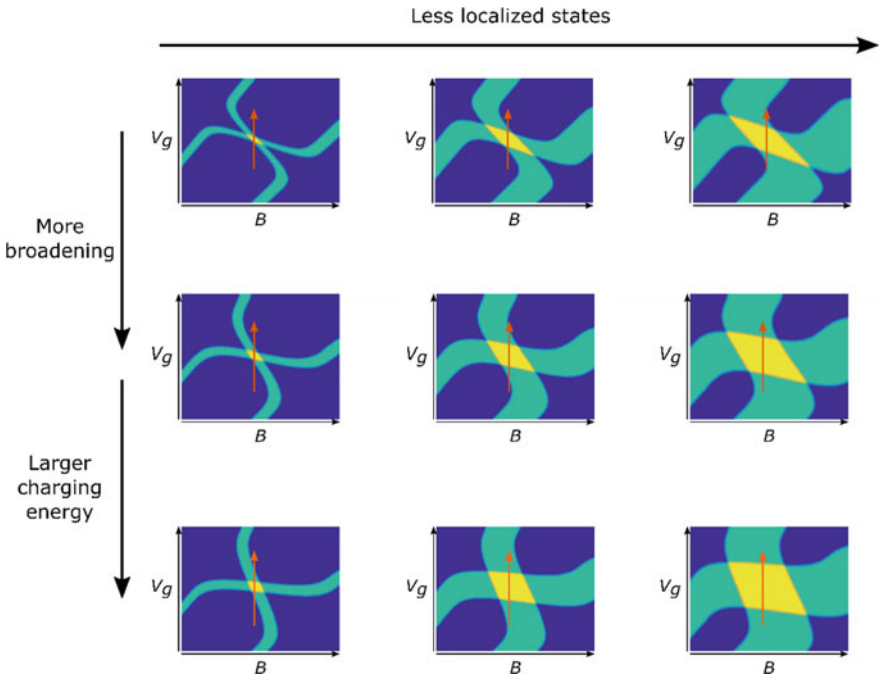

Fig. 3.13 Rxx on the Vg-B plane in the LLs crossing region for various amounts of localized states, LLs broadening and inter-subband charging energy

crosses the Fermi energy closer to the left gate and the LL of SB_2 crosses the Fermi energy closer to the right gate, resulting in a lateral distance between the two edge modes (Fig. 3.14c, left image).

This gives us an important tool to control the coupling between the edge modes in a given device, as will be demonstrated in Sect. 7.

3.6 Fractional Helical Modes

We turn now to the fractional regime. Figure 3.15a shows a zoom on the R_{xx} color plot of *DQWa* around the (2, 0) → (1, 1) transition. Points A (yellow) and B (red), which stand for $\left(\frac{4}{3}, 0\right)$ and $\left(1, \frac{1}{3}\right)$, respectively, allow an intersection of counter-propagating, $\nu = \frac{1}{3}$ edge modes with opposite spins (Fig. 3.15b). Just as in the integer case, to confirm the existence of the correct edge mode structure, a current of 1nA is injected at S_1 (S_2) and its reflected part, $I_{S1\to D1}$ ($I_{S2\to D2}$), is plotted in Fig. 3.15c. The left gate voltage, V_{LG}, is tuned to point A (yellow) of Fig. 3.15a, while the right gate voltage, V_{LG}, is scanned along the black arrow shown in the figure. Indeed in the appropriate range of V_{RG}, the currents $I_{S1\to D1}$ and $I_{S2\to D2}$ are both found to be 0.25 nA (Fig. 3.15c, green regions).

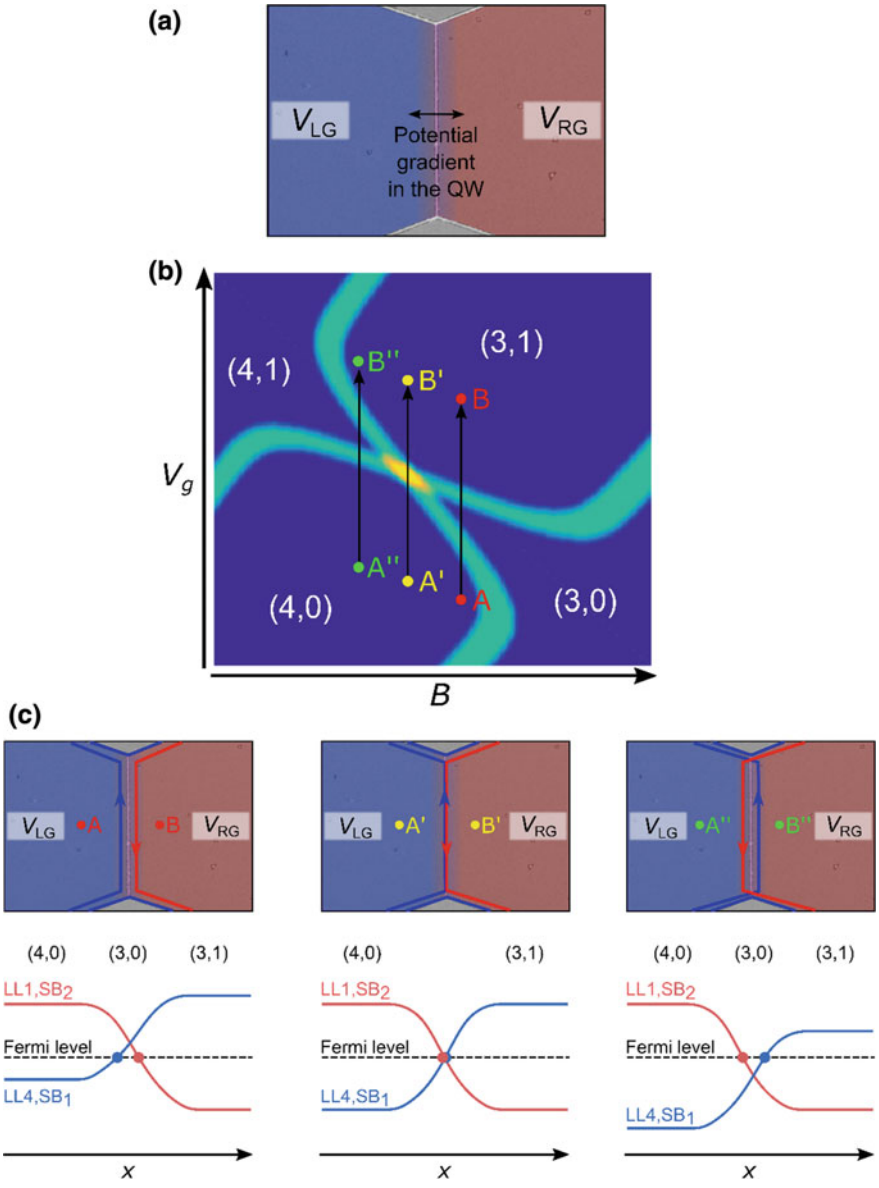

Fig. 3.14 Manipulating the lateral distance between counter-propagating edge modes

Note that while $I_{S2\to D2}$ is not affected by the propagation length, $I_{S1\to D1}$ decreases slightly as the propagation length increases. However, as shown in Fig. 3.15a there is no corresponding increase in the transmitted current, $I_{S1\to D2}$. Moreover, as shown in Fig. 3.16b, a non-zero R_{XX} is found in the right half-plane in

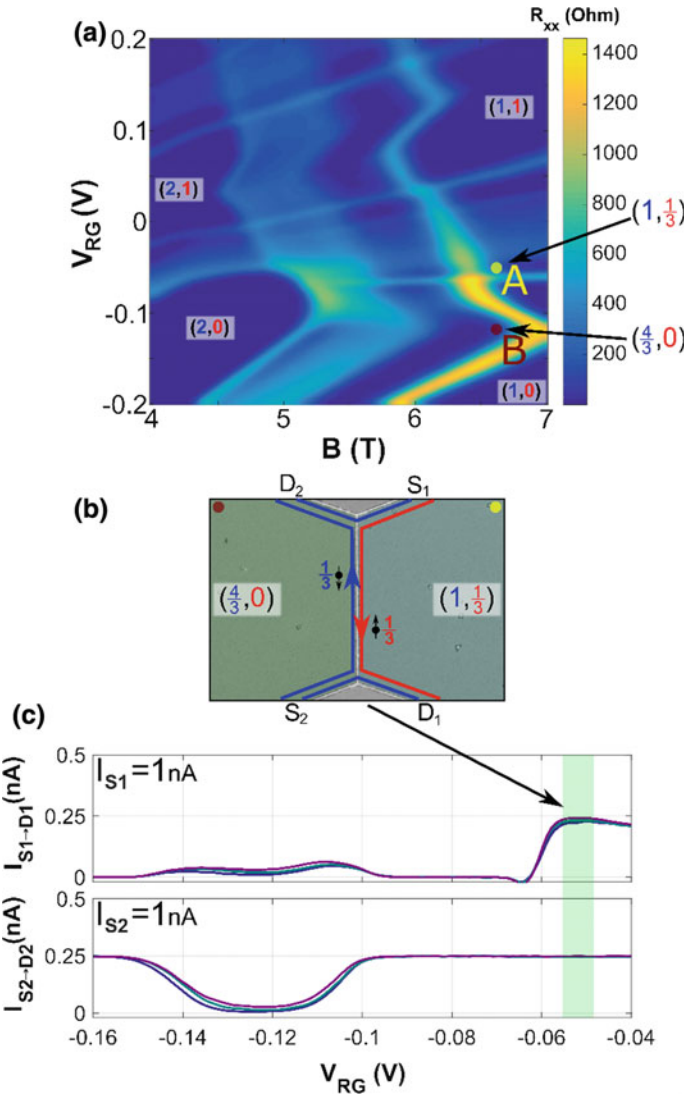

Fig. 3.15 Fractional helical modes

the corresponding gate voltage range. Therefore, we attribute the decrease in $I_{S1\to D1}$ to current flow through the bulk (and from there to other grounded contacts) rather than to tunneling between the edge modes. Note that this is consistent with the fact that when current is injected from contact S_2, the reflected current $I_{S2\to D2}$ is not affected by the length of propagation (Fig. 3.15c).

To the best of our knowledge, this is a first demonstration of fractional helical modes.

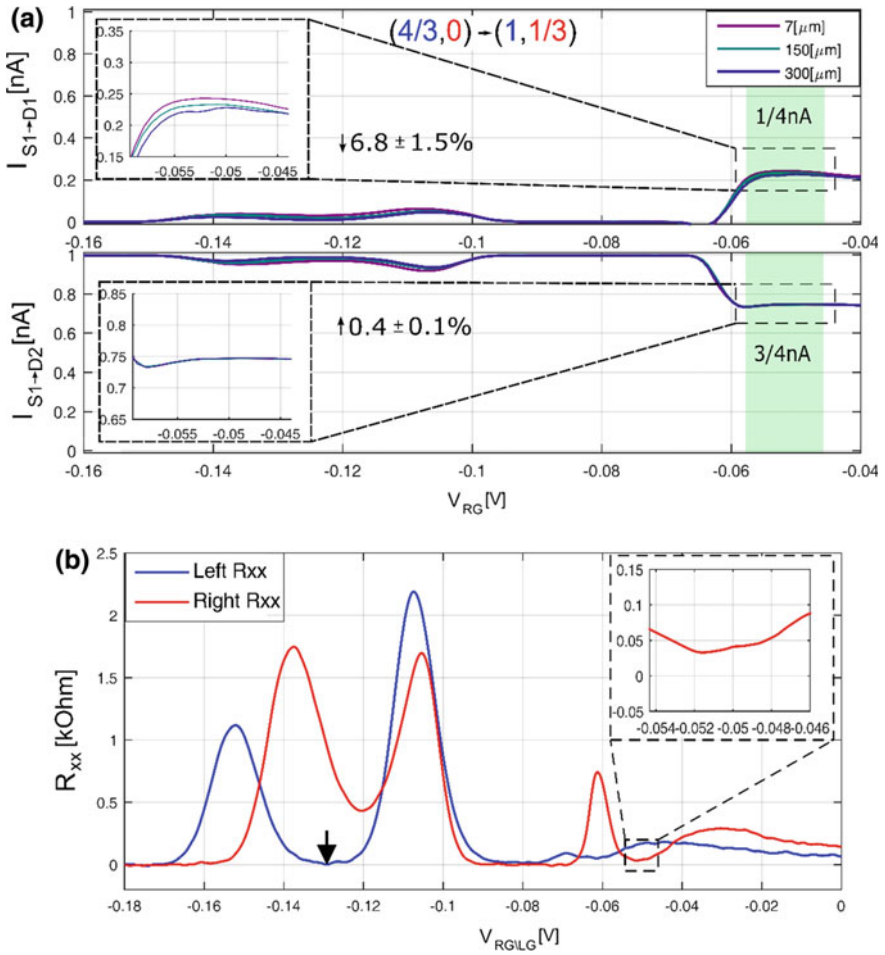

Fig. 3.16 Further measurements on fractional helical modes showing the absence of inter-mode tunneling in the fractional helical edge modes. **a** While there is a slight decrease in $I_{S1\rightarrow D1}$ as the propagation length increases, there is no corresponding increase in $I_{S1\rightarrow D2}$. Moreover, **b** shows that the right half-plane exhibits a non-zero R_{xx} in the corresponding gate voltage range and therefore, we attribute the decrease in $I_{S1\rightarrow D1}$ to current flow through the bulk rather than to tunneling between the edge modes

3.7 Engineering Hole-Conjugate FQHE Edge Modes

The edge modes in the QHE reveal an even richer physics than integer and fractional charge excitations. In the 1990s, several theoretical works predicted that the edge structure of the so called particle-hole conjugate states can be composed of more than one edge mode per quantum state and include *downstream* (along the chirality) as well as *upstream* (against the chirality) modes [4, 5]. The particle-hole

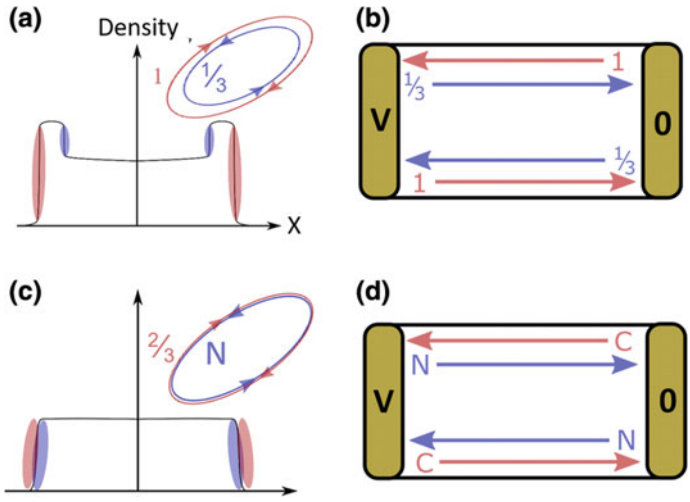

Fig. 3.17 The 2/3 hole-conjugate state and its synthetized form. **a** The unequilibrated v = 2/3 state; composed of two counter-propagating chiral modes: a downstream v = 1 mode and an upstream v = 1/3 Laughlin excitation mode. Red and blue represent electron density profile of independent v = 1 and v = 1/3 modes at the edges respectively. **b** Equivalent two-terminal conductance in the unequilibrated regime. **c** Inter-mode scattering results in edge density profile reconstruction: coexistence of a downstream v = 2/3 mode and an upstream neutral mode. **d** Equivalent two-terminal conductance in the equilibrated regime

conjugate states are states such as $\nu = 2/3, 3/5, 4/7$, etc., which can be explained by particle-hole symmetry from the Lauphlin-like states $\nu = 1/3, 2/5, 3/7$, etc. The most famous such state is the $\nu = 2/3$ state, which can be constructed from a full LL (i.e. $\nu = 1$) and a $\nu = 1/3$ Lauphlin state of holes. In 1991, MacDonald showed that the edge of this state is expected to support two counter-propagating edge modes—an upstream mode carrying charge conductance of $1e^2/h$ (electron excitations), and a downstream mode carrying charge conductance $1/3(e^2/h)$ ($e/3$ anyonic excitations) [6] (Fig. 3.17a). However, this picture predicts that the two-terminal conductance in the $\nu = 2/3$ should be $G_{2T} = 4/3(e^2/h)$ (Fig. 3.17b), while all experimental works that followed McDonald's work consistently observed $G_{2T} = 2/3(e^2/h)$.

To explain this, Kane, Fisher and Polchiski (KFP) added random tunneling (due to disorder), accompanied by Coulomb interaction, to the counter-propagating 1 and 1/3 edge mode model. As KFP showed, this leads to a phase transition, which results in a single downstream charge mode carrying a charge conductance of 2/3 (e^2/h), and a so called upstream *neutral mode*—an edge mode carrying only heat conductance with no charge [7] (Fig. 3.17c, d). 16 years later, in 2010, such neutral modes where successfully detected [8] and studying them have become a new research frontier.

Nevertheless, the KFP transition itself, namely counter-propagating 1 and 1/3 modes which transition to counter-propagating 2/3 and neutral modes as a tunneling

increases, was never demonstrated and probed experimentally. The main difficulty is that in the $\nu = 2/3$ FQHE state, the edge modes are almost always in the tunneling dominated phase. Moreover, recent theoretical and experimental works showed that the $\nu = 2/3$ edge structure may be more complicated and involve two downstream 1/3 charge modes as well as two upstream neutral modes [9, 10], making it even more difficult to interpret experimental results. An experimental setup that allows starting from clean counter-propagating 1 and 1/3 edge modes and controllably coupling them, so that they transition to the 2/3 and neutral edge modes, is therefore highly desired. Such an experiment is of interest, not just to confirm the KFP picture, but even more importantly, since a new theoretical work expanded the KFP picture and demonstrated that the phase transition can have different fundamental nature depending on the strength of the inter-mode interactions [11]. The two subbands quantum Hall system allows an elegant way to construct such an experimental setup.

3.7.1 Experimental Setup

The device used, denoted by *Device C*, is shown in Fig. 3.18a. Three horizontal top-gates separate the 2DEG plane to three regions: upper, center and lower, with each gate controlling the filling factor in the 2DEG underneath it. As illustrated in the figure, when the filling factors under the upper (or lower) gate and center gate are tuned to $\nu = (1, 1)$ and $\nu = (4/3, 0)$, respectively, the desired counter-propagating edge modes are obtained.

Device C contains a series of ohmic contacts, placed on the interface between the top-gates and separated by varying distances. Each source (S in Fig. 3.18a) contact was placed in the middle between two grounded Drains (D in Fig. 3.18a), so that the two-terminal conductance between source and ground can be measured for several source-drains separation lengths. This allows probing the edge mode conductance as a function of the propagation length, L. In addition, as explained in Sect. 5, by varying the magnetic field, the lateral distance, d, between the two edge modes can be varied, to affect the inter-mode coupling strength. For the purpose of this experiment, a new DQW heterostructure was grown, denoted by *DQWc*. This DQW has a thinner AlAs barrier (of two monoloayers) to allow for a relatively large range of L and d values inside the phase transition (where $2/3 (e^2/h) < G_{2T} < 4/3(e^2/h)$).

Figure 3.18b shows the R_{xx} versus B and V_g color plot for *DQWc*. The figure is split to two since the two measurements were taken separately. *DQWc* has a significantly higher mobility, which allows for more FQHE states to develop and to much larger FQHE plateaus ($R_{xx} = 0$ regions). In addition, since due to the thinner barrier in the center of the quantum well, the spatial overlap between the two SBs is larger, leading to higher tunneling and therefore to a gap opening in the crossing of LL2 of SB_1 and LL1 of SB_2 (avoided crossing).

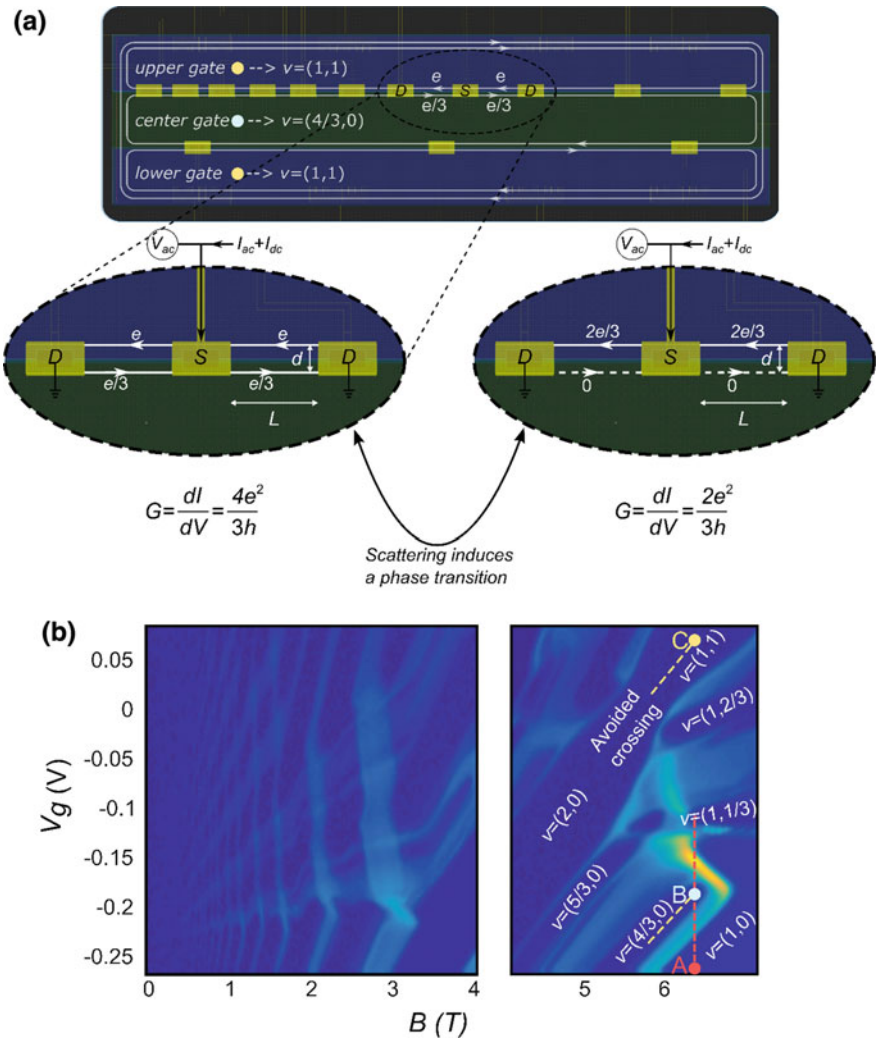

Fig. 3.18 Device C. Engineering hole-conjugate FQHE edge modes

3.7.2 Differential Conductance Measurements

The upper gate of *Device C* is tuned to point C (yellow point) in Fig. 3.18b, so that the filling factor underneath is $\nu = (1, 1)$. The center gate is then scanned along the red dashed line in the figure so that it passes from point A (red), where $\nu = (1, 0)$, and through point B (blue), where $\nu = (4/3, 0)$. The two-terminal conductance as a function of the center gate voltage, is shown in Fig. 3.19a for various propagation lengths, L. The highlighted region in red corresponds to the center region being at

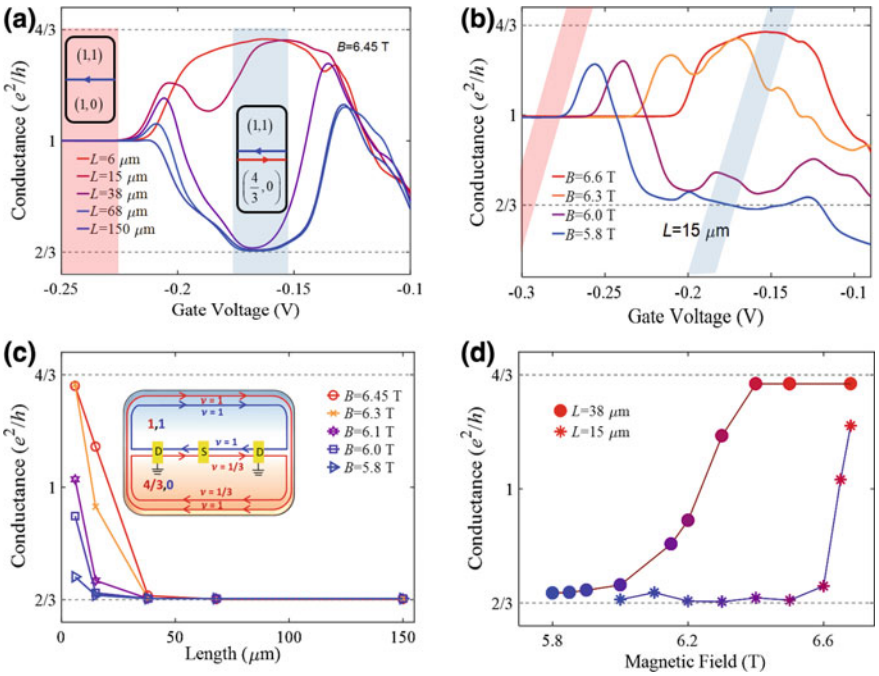

Fig. 3.19 Length and magnetic field dependent two-terminal conductance. **a** Two-terminal conductance versus center top-gate voltage for different propagating lengths at B = 6.45T. The upper region is set to (1, 1), and the center region in the ranges highlighted by red and blue areas are tuned to (1, 0) and (4/3, 0), respectively. In blue area, a v = 1 and a v = 1/3 counter-propagating chiral modes coexist at the interface, and the conductance decreases from 4/3(e^2/h) to 2/3(e^2/h) as channel length increases from 6 to 150 μm. In red area, the conductance is e^2/h is length independent due to a single a v = 1 chiral mode at the interface. **b** Two-terminal conductance versus propagating length at different magnetic fields, with the center region is tuned to (4/3, 0). **c** Two-terminal conductance of a 15 μm long channel as a function of center gate voltage for a range in field 5.8T < B < 6.6T. The colored areas are as above. **d** Dependence of the two-terminal conductance on the magnetic field for propagating length L=38 and 15 μm. With decreasing the magnetic field the two-terminal conductance evolves from 4/3(e^2/h) to 2/3(e^2/h)

filling (1, 0), thus supporting a single downstream integer mode with the conductance equals e^2/h—independent of the propagation length. Once the gate voltage of the center region is increased, placing its filling at ν = (4/3, 0), an evolution of the two-terminal conductance, from $G_{2T} = 4/3(e^2/h)$ at short distance (6 μm) to $G_{2T} = 2/3(e^2/h)$ at long distance (150 μm) is observed (highlighted in blue in Fig. 3.19a). The full development of the phase transition from the fully decoupled phase to the fully coupled phase is observed.

Figure 3.19b shows the two-terminal conductance as a function of the center gate voltage, with a fixed propagation length, L = 15 μm, for various magnetic fields. The red and blue regions correspond, again, to center region filling factors (1, 0) and (4/3, 0), respectively. Note that to keep these filling factors constant as the

magnetic field changes, the gate voltage must also change, as shown by the dashed yellow lines in Fig. 3.18b. Thus, the colored regions in Fig. 3.19b are tilted accordingly. Similar to the case in Fig. 3.17a, in the red region only a single integer mode propagates along the edge and thus the conductance is quantized at e^2/h with no magnetic field dependence. In the blue region, however, strong magnetic field dependence is observed, which is attributed to the strong effect of the magnetic field on the inter-mode coupling. In the high field region, the two edge modes are fully decoupled and the conductance approaches $G_{2T} = 4/3(e^2/h)$, while at lower fields, the edge modes are coupled and the conductance approaches $G_{2T} = 2/3(e^2/h)$.

Figures 3.17c shows how the two-terminal conductance in the counter propagating modes configuration develops as a function of propagation length (i.e. the development along the blue region of Fig. 3.19a), for various magnetic fields. At high magnetic field, the full transition from $G_{2T} = 4/3(e^2/h)$ to $G_{2T} = 2/3(e^2/h)$ is observed, while at lower fields the two modes are coupled even for the shortest propagation length of $L = 6$ μm.

Figure 3.19d shows how the two-terminal conductance in the counter propagating modes configuration develops as a function of magnetic field (i.e. the development along the blue region of Fig. 3.19b), for various two different propagation lengths. For the short propagation length, $L = 15$ μm, the full transition is observed, with nice conductance plateaus at $G_{2T} = 4/3(e^2/h)$ and $G_{2T} = 2/3(e^2/h)$. For the longer propagation length, $L = 38$ μm, the conductance does not reach $G_{2T} = 4/3(e^2/h)$, even for the highest magnetic field, $B = 6.6$T. These results indicate that magnetic field serves as a powerful tool for controlling the inter-mode coupling.

3.7.3 Noise Measurements and Neutral Modes

As mentioned above, the tunneling dominated, $G_{2T} = 2/3(e^2/h)$, state is expected to consists of a downstream charge mode accompanied by a diffusive upstream neutral mode [7, 11]. The experimental setup used to measure such a neutral mode is sketched in Fig. 3.20a. The current that is injected to the source contact propagates toward the grounds, while the voltage noise is measured 38 μm away from the source contact, in A1 and in A2. This voltage noise indicates the presence of a heat carrying neutral mode. The measurements were performed in the equilibrated regime; namely, with $G_{2T} = 2e^2/3\ h$ and thus charge propagating only downstream (towards A2).

Noise was measured at contact A1 for different magnetic field strengths (Fig. 3.20b). The noise increased monotonically with the injected DC current and tended to saturate at higher current values. As the magnetic field increased (away from B_c), the inter-mode interaction got weaker (Fig. 3.22), and the measured excess-noise increased (Fig. 3.20b). The observed noise is a manifestation of the upstream diffusive neutral mode excited by the "hot spot" at the back of the source contact (Fig. 3.20a). With the magnetic field increasing, the equilibration length,

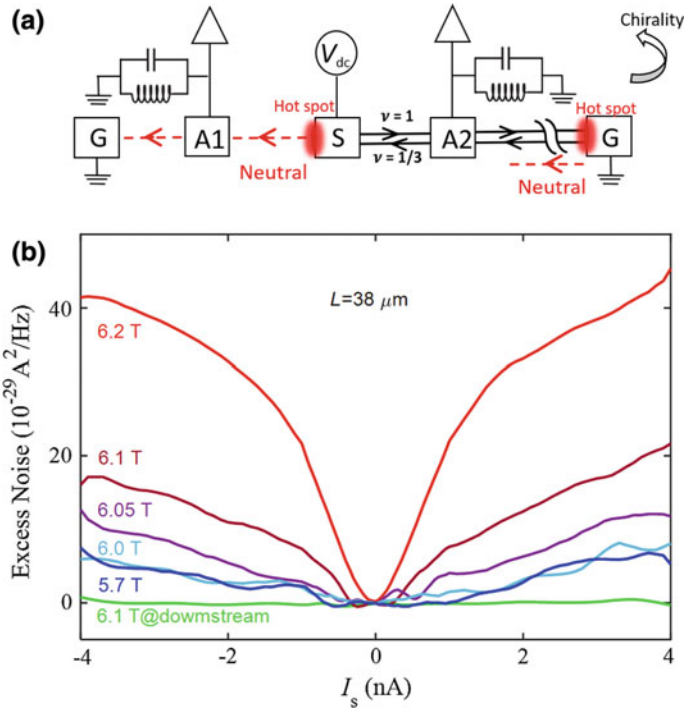

Fig. 3.20 Noise measurement setup and experimental results. **a** Schematic diagram of noise measurement circuit. Current is injected from source S and the upstream and downstream noises are measured by a spectrum analyzer through amplifier contacts A1 and A2 respectively, followed by an LC circuit at a center frequency f0 = 1.3 MHz, and amplified by two home-made (cooled) voltage pre-amplifiers, each followed by a commercial, room temperature, voltage amplifier (NF-220F5). **b** Upstream excess noise collected from contacts A1 as a function of Is at different magnetic fields, whose amplitude initially reduces as decreasing magnetic field, then keep stable at B < 6T. Green line represents the Is-independent downstream excess noise at B = 6.1T

needed to fully excite the neutral mode, increases too, thus facilitating a shorter propagating distance of the heat to reach the amplifier at A1. No sizeable excess-noise was detected at A2, which is attributed to the much larger distance between the "hot spot" at G (on the right) and A2 (108 μm). As expected, measurements performed when the interface was hugged by ν = (1, 1) and ν = (1, 0), did not find any excess noise, either in A1 or in A2.

3.7.4 Non-equilibrium Measurements

While the above measurements agree well with theory, when adding a bias to the measurement a striking result is observed. Figure 3.21a shows the differential conductance measured as a function of voltage bias, V_{SD}, for several different

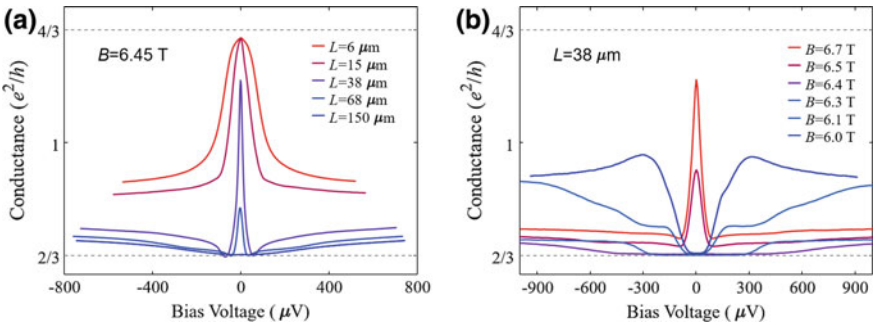

Fig. 3.21 Differential conductance as a function of bias for **a** different counter-propagation lengths, L, and **b** different magnetic fields leading to different lateral distance, d

values of the propagation length, L, keeping the magnetic field fixed at B = 6.45T. When at zero bias the edge modes are not in the fully equilibrated phase (*i.e.* $G_{2T} > 2/3(e^2/h)$), as the bias is increased, the conductance initially decreased sharply (up to $\sim$150 μV and less), forming a zero-bias conductance peak. At very short propagation lengths (L = 6 and 15 μm), the conductance does not drop all the way to $G_{2T} = 2/3(e^2/h)$ and instead starts dropping very slowly at higher voltage bias. For longer propagation lengths (L = 38 and 68 μm), the conductance drops all the way to $2/3(e^2/h)$ (at a range $V_{DC} \sim$ 35–60 μV), followed by a soft increase with incasing DC bias. For the longest distance (L = 150 μm), for which the system is in the fully equilibrated phase a zero-bias (i.e. $G_{2T} = 2/3(e^2/h)$, the conductance increases smoothly with bias.

Figure 3.21b shows the differential conductance as a function of the DC bias for several magnetic fields at a propagation length of L = 38 μm. At higher B (weak inter-mode coupling), a similar zero-bias conductance peak appears. At lower B, however, the conductance, $\sim 2/3(e^2/h)$, was flat around zero bias; but experienced a rather steep increase with a shoulder-like structure as the bias increased. The critical bias, where the conductance shoulders appeared, increased gradually with lowering the magnetic field.

We therefore observe a unique bias behavior. It seems that the inter-mode tunneling is strongly suppressed at zero bias, as well as at some finite bias voltage that is highly dependent on the magnetic field. As the spin orientations of the 1 and 1/3 modes in our set up are opposite, such behavior might be related to the energy required for a spin-flip. Yet, interpretation of the behavior of the non-linear differential conductance is not trivial and requires more studies.

3.8 Future Prospect: Edge Mode Interferometers in the Two Subbands QHE System

The 1D edge modes of the QHE together with the verity of device architecture possibilities in GaAs samples provide a great playground for interference experiments. Mach-Zehnder (MZ) and Fabty-Perot (FP) interferometers can be designed to study electronic interference and entanglement as well as the effects of interactions which are not present in other interference experiments platforms, such as optical systems. Moreover, in the FQHE regime interference was predicted to provide signature of anyonic statistics [12–16]. Unfortunately, in the FP geometry Coulomb interactions dominates the interference pattern and prevents observation of such signature [17], while in the MZ geometry interference was simply never observed in the FQHE regime.

There are two important differences between the MZ and FP geometries in the QHE regime which may hint on possible promising directions. First, due to fabrication limitations, the MZ cannot be made as small as the FP. Since the FP shows interference in the FQHE regime only for small size ($\sim 2 \times 2$ μm or smaller), it is possible that if the MZ was made smaller, fractional interference could be detected. Second, while in the MZ geometry there is an ohmic contact inside the interference area, the FP is free from such a contact. In fact, when an ohmic contact is deliberately added inside the FP area, the effect of Coulomb interaction significantly weakens [18, 19], however at the same time, there is no sign of fractional interference. One possible issue that the contact can introduce is density variations in its vicinity. This effect, which can be quite strong can change completely the filling factor in the MZ area or lead to several different filling factors in it. Therefore, it is highly desirable to remove the ohmic contact from the MZ in an attempt to detect fractional interference.

As an outlook for the future and as a last demonstration of some of the possibilities of the two subband QHE platform, we now show how it allows making a significantly smaller than usual MZ with no ohmic contact inside its interference area. These days, we are preparing the devices we discuss below and performing some preliminary measurements needed to pursue this direction.

The geometry of the device, together with the appropriate filling factors under each gate and with the edge modes demonstration is shown in Fig. 3.22. For simplicity, we show the case for integer edge modes, but this can be done with fractional modes as well. Two edge modes of different subbands are brought to co-propagate close to each other for a certain distance L_t. Along this distance, tunneling occurs between the edge modes so that this region acts as the beam splitter of the MZ. The two edge modes are then separated and encircle an Aharonov-Bohm flux and then brought together to mix again. If current is injected from, say contact S_1 an interference pattern should be observed in both D_1 and D_2, as indicated in the figure. Since no ohmic contact is needed inside the interference area, this area can be made very small.

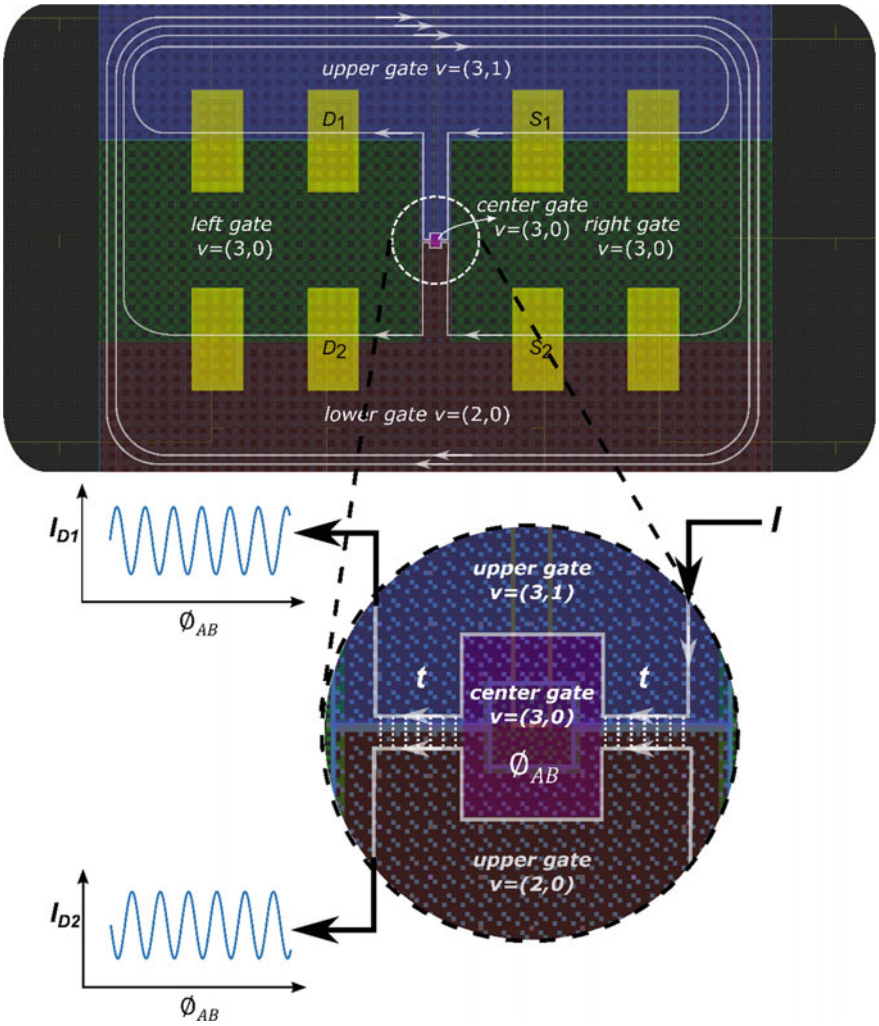

Fig. 3.22 MZ interferometer with a two SB QHE system

Another interesting feature this MZ provide is that by changing the filling factors configuration the edge modes could be made to counter-propagate (instead of co-propagate). This then form a FP interferometers and thus, MZ and FP physics could be compared in the same device.

References

1. Haug, R.J., MacDonald, A.H., Streda, P., von Klitzing, K.: Quantized multichannel magnetotransport through a barrier in two dimensions. Phys. Rev. Lett. **61**, 2797–2800 (1988)
2. Nuebler, J., et al.: Quantized ν = 5/ 2 State in a two-subband quantum hall system. Phys. Rev. Lett. **108**, 46804 (2012)
3. Liu, Y., et al.: Evolution of the 7/2 fractional quantum hall state in two-subband systems. Phys. Rev. Lett. **107**, 266802 (2011)
4. Wen, X.G.: Chiral Luttinger liquid and the edge excitations in the fractional quantum Hall states. Phys. Rev. B **41**, 12838–12844 (1990)
5. MacDonald, A.H.: Edge states in the fractional-quantum-Hall-effect regime. Phys. Rev. Lett. **64**, 220–223 (1990)
6. Johnson, M., MacDonald, A.: Composite edges in the ν = 2/3 fractional quantum Hall effect. Phys. Rev. Lett. **67**, 2060–2063 (1991)
7. Kane, C.L., Fisher, M.P.A., Polchinski, J.: Randomness at the edge: theory of quantum Hall transport at filling ν=2/3. Phys. Rev. Lett. **72**, 4129–4132 (1994)
8. Bid, A., et al.: Observation of neutral modes in the fractional quantum Hall regime. Nature **466** (2010)
9. Sabo, R., et al.: Edge reconstruction in fractional quantum Hall states. Nat. Phys. **13**, 491–496 (2017)
10. Wang, J., Meir, Y., Gefen, Y.: Edge reconstruction in the ν = 2/3 fractional quantum hall state. Phys. Rev. Lett. **111**, 246803 (2013)
11. Protopopov, I.V., Gefen, Y., Mirlin, A.D.: Transport in a disordered ν = $2/3$ fractional quantum Hall junction. Ann. Phys. (N. Y.) **385**, 287–327 (2017)
12. de Chamon, C., Freed, D.E., Kivelson, S.A., Sondhi, S.L., Wen, X.G.: Two point-contact interferometer for quantum Hall systems. Phys. Rev. B **55**, 2331–2343 (1997)
13. Law, K.T., Feldman, D.E., Gefen, Y.: Electronic Mach-Zehnder interferometer as a tool to probe fractional statistics. Phys. Rev. B **74**, 45319 (2006)
14. Fradkin, E., Nayak, C., Tsvelik, A., Wilczek, F.: A Chern-Simons effective field theory for the Pfaffian quantum Hall state. Nucl. Phys. B **516**, 704–718 (1998)
15. Das Sarma, S., Freedman, M., Nayak, C.: Topologically protected Qubits from a possible Non-Abelian fractional quantum Hall state. Phys. Rev. Lett. **94**, 166802 (2005)
16. Stern, A., Halperin, B.I.: Proposed experiments to probe the Non-Abelian ν = 5/2 quantum Hall state. Phys. Rev. Lett. **96**, 16802 (2006)
17. Ofek, N., et al.: Role of interactions in an electronic Fabry-Perot interferometer operating in the quantum Hall effect regime. Proc. Natl. Acad. Sci. U. S. A. **107**, 5276–5281 (2010)
18. Choi, H.K., et al.: Robust electron pairing in the integer quantum hall effect regime. Nat. Commun. **6**, 7435 (2015)
19. Sivan, I., et al.: Observation of interaction-induced modulations of a quantum Hall liquid's area. Nat. Commun. **7**, 12184 (2016)

Chapter 4
Summary

We have developed a two subband quantum Hall system that can be used to manipulate integer and fractional quantum Hall edge modes in ways which were unachievable before. Using this system we demonstrated the formation of robust helical modes and, for the first time to the best of our knowledge, fractional helical modes. These modes are highly desirable for creating Majorana zero modes and parafermionic zero modes that are the basic building blocks for topological quantum computations. While most platforms used by now in an attempt to realize these quasiparticles suffer from difficulties in robustness, fabrication methods and scalability, our platform, which is implemented in GaAs/AlGaAs heterostructures, provide evident advantages in these respects. Moreover for parafermionic zero modes it is almost essential to use the edge modes of the fractional quantum Hall effect which are most easily obtained in such heterostructures. Byond helical modes, we have used the new system to create compounded integer-fractional edge modes and probed the Kane-Fisher-Polchinski phase transition. We discovered interesting bias dependence which points to a strong suppression of tunneling at zero bias as well as an unexpected energy scale in the system, results which we are interpreting these days. We have demonstrated control over edge mode coupling, distance and spin and have started working towards a realization of an extremely small size Mach-Zehnder interferometer with no ohmic contact in its center.

Y. Cohen, *A New Platform for Edge Mode Manipulations in the Quantum Hall Effect*, Springer Theses, https://doi.org/10.1007/978-3-030-05943-9_4